Four-Charged-Particle Final States from the Interaction of 2.7-GeV/c π^+ on Deuterium*

R. J. MILLER,† S. LICHTMAN, AND R. B. WILLMANN
Purdue University, Lafayette, Indiana 47907
(Received 15 October 1968)

Reactions leading to four nonstrange, charged particles from the interaction of 2.7-GeV/c π^+ on deuterium have been studied. Only events containing at least one visible stopping proton track were included. The spectator model of the π^+d interaction has been examined and found to be a good approximation. This model not only gives a good description of the final state of the spectator nucleon, but is also supported by the similarity of such reactions as $\pi^+d \to pp\rho^0$ and $\pi^-p \to n\rho^0$. Meson (M) resonance production in the reaction $\pi^+d \to ppM$ is prominent, including $\eta(0.21\pm0.04$ mb), $\omega(0.80\pm0.08$ mb), $\rho(2.20\pm0.25$ mb), $f(0.51\pm0.20$ mb), $A_1(0.17\pm0.10$ mb), $A_2(0.14\pm0.08$ mb), and $\eta'(0.05\pm0.02$ mb) (errors are statistical). The baryon resonance $\Delta(1238)$ is also observed to be produced in a variety of reactions. The ρ and ω production processes have been examined in some detail, including a determination of the spin density matrix elements. Also, the 3π system in the $pp\pi^+\pi^-\pi^0$ final state has been studied at energies near the A_1 and A_2 masses in an attempt to separate these particles from the several other processes contributing to this final state. The results of a spin-parity analysis of the A mesons are presented.

I. INTRODUCTION

THIS is a report of an examination of several of the final states from the interaction of positive π mesons at 2.7-GeV/c laboratory momentum with stationary deuterons. The final states described are those with four charged, strangeness-zero particles (four-prong events). The main purpose of the experiment was to study the neutral resonances decaying into two or three pions, in particular, the ρ^0 in the $pp\pi^+\pi^-$ final state and the η, ω, A_1, and A_2 in the $pp\pi^+\pi^-\pi^0$ final state.

The data for this experiment were collected at the Lawrence Radiation Laboratory, Berkeley, in collaboration with experimenters from the University of California and the University of Illinois.

A secondary beam from the Bevatron was separated to give better than 95% π^+ at the 72-in. bubble chamber.[1] Approximately 85 000 pictures were taken at the 2.7-GeV/c momentum.

Sections II and III of this paper describe the procedure used in scanning and measuring the selected sample of events and the method by which these events were assigned to a particular final state. In Sec. IV, distributions of the spectator proton are compared with those expected from the impulse model of the π^+d interaction. The final state $pp\pi^+\pi^-\pi^0$ is described in Sec. V with special attention given to the mesons in the $\pi^+\pi^-\pi^0$ state. Section VI contains a description of the $pp\pi^+\pi^-$ final state and a comparison of the details of ρ meson production in π^+d and π^-p interactions. The $p\pi^+\pi^+\pi^-n$ and $pp\pi^+\pi^-$MM states are discussed in Secs. VII and VIII, respectively. The method of determining the cross-section estimates is described in Sec. IX.

II. SCANNING AND MEASURING

The scanning criteria were designed to select probable interactions on the neutron of the deuterium nucleus, with the proton a spectator particle. The final states discussed here are taken from the events having three positive and one negative track leaving the vertex. At least one of the positive particles was required to be a proton which stopped within the bubble chamber.

For the purpose of determining cross sections, a portion of the film was also scanned for three-prong events associated with invisible spectator protons.

All of the events which were recorded during the scan met several other criteria. None of the tracks were obvious electrons or positrons. There were no neutral strange particles (V's) associated with the event. The beam track was parallel within 2° to the other beam tracks in the frame and was not obviously dissimilar in curvature. A restricted fiducial volume was used to ensure that all tracks would be sufficiently long for measuring. The over-all scanning efficiency for the four-prong events, determined from an independent second scan of about half of the film, was 92%.

The events were measured with either a scanning-measuring projector or a digitizing microscope on line to an IBM 7044–1401 computer system.[2] The spatial reconstruction of the event and the reduction of the raw track data to momentum and angles was done with the programs PANAL and PANG, respectively.[3] These programs utilized the best two of the three stereo views for geometric reconstruction.

During most of the measuring period a version of the Berkeley three-view reconstruction program TVGP was used on-line.[4] However, subsequent links in this three-view system, in particular the fitting programs, were

* Work supported in part by the U. S. Atomic Energy Commission.
† Present address: Rutherford High Energy Laboratory, Berkshire, England.
[1] Some aspects of this experiment are described in more detail in R. J. Miller, thesis, Purdue University, 1969 (unpublished).
[2] P. G. Davey, R. I. Hulsizer, W. E. Humphrey, J. H. Munson, P. R. Ross, and A. J. Schwemin, Rev. Sci. Instr. 35, 1134 (1964).
[3] A. H. Rosenfeld, University of California Lawrence Radiation Laboratory Report No. UCRL-9099, 1961 (unpublished).
[4] T. B. Day, reprint of seminar at Argonne National Laboratory, 1967 (unpublished).

TABLE I. The final-state hypotheses considered. N_3 and N_4 are the number of events in the samples with invisible and visible spectator tracks, respectively.

Hypothesis	Constraint class	N_3	N_4
$\pi^+d \to d\pi^+\pi^+\pi^-$	4	3	438
$\pi^+d \to d\pi^+\pi^+\pi^-\pi^0$	1	0	173
$\pi^+d \to d\pi^+\pi^+\pi^-\mathrm{MM}(>2\pi^0)$	0	2	18
$\pi^+d \to p_s p\pi^+\pi^-$	4	570	3256
$\pi^+d \to p_s p\pi^+\pi^-\pi^0$	1	730	3977
$\pi^+d \to p_s p\pi^+\pi^-\mathrm{MM}(>2\pi^0)$	0	289	1840
$\pi^+d \to p_s\pi^+\pi^+\pi^-n$	1	293	1917
$\pi^+d \to p_s\pi^+\pi^+\pi^-\mathrm{MM}(>n\pi^0)$	0	221	1574

not ready for use, so that TVGP was used only as an on-line measurement quality check as far as this experiment was concerned.

A sample of beam tracks was measured to determine the average and spread of the beam momentum and to determine limits of acceptance for beam angles and position. For events with short or poorly measured beam tracks, the beam momentum was actually better known than the single measurement would indicate. For this reason the weighted average of the measured value and the "beam average" value of the beam momentum was used for the fitting of each event. The limits on beam angles and position were set to prevent contamination from particles which scattered before entering the chamber.

III. RESOLVING THE FINAL STATES

The measured momenta and angles for each event were fitted to each of the hypotheses listed in Table I. The fitting program used was a version of the Berkeley program PACKAGE.[5] A constrained fit was considered acceptable if the χ^2 of the fit was below the 1% confidence level. The missing mass (MM) hypotheses were accepted only if the value of MM+3Δ MM was larger than the minimum mass of two missing neutrals.

The three-prong events were also fitted to the same hypotheses listed in Table I. However, some assumption was required concerning the unseen charged particle (p_s) in these cases. The three-momentum vector for that particle was set equal to zero with errors $\Delta p_x = \Delta p_y = 30$ MeV/c, $\Delta p_z = 40$ MeV/c. These values correspond to the mean and standard deviation expected from the Hulthén wave-function description of the deuteron with typical measurement uncertainties folded in.

After the fitting, each event was reexamined on the scan table and all mass assignments were checked for consistency with track bubble densities. Events having no acceptable hypothesis at this stage were given a special examination. If the event was obviously pathological (e.g., a secondary interaction near the vertex), it was classed as unmeasureable and eliminated from the sample; otherwise, it was remeasured. If the event was still unacceptable after the second attempt, it was assigned to a "no fit" category. Approximately 88% of the events had only one acceptable mass assignment for the visible particles after passing the ionization examination.

The remaining ambiguities were resolved by the following prescription:

(a) If the constraint classes of the competing hypotheses were different, the event was put in the most highly constrained sample (5728 events).

(b) If the constraint classes were equal (but not zero), the event was assigned to the hypothesis with the lowest χ^2 (223 events).

(c) If the competing hypotheses were unconstrained (multiple missing neutrals), the ambiguity was unresolvable and these events were not added to any sample (112 events).

The justification of the first most definitive rule is essentially the fact that it is much harder for an event to fake a highly constrained hypothesis than a poorly constrained one. A quantitative examination of this difference is given in Ref. 1. In no case is the number of misassigned events expected to be greater than 2% of the final-state sample.

IV. SPECTATOR PROTON

The usual assumption which is made for the π^+d interaction, the impulse approximation, treats the initial state as πN with the other nucleon a spectator.[6] There are at least two ways to check the validity of the spectator model within this experiment. The first, most convincing method involves a direct comparison of results obtained using the impulse model with those obtained in an experiment where this approximation is not needed. Since the strong interaction does not depend on the orientation in isospin space, one can compare, for example, the reaction $\pi^+n(p) \to (p)p\pi^+\pi^-$ with the reaction $\pi^-p \to n\pi^-\pi^+$, where the parentheses in the first reaction indicate the spectator. This will be done in Secs. VI and VII.

Another approach is to examine the final state of the spectator proton. In the approximation that this particle is a spectator, its momentum distribution in the initial and final states should be the same. A commonly accepted wave function for the deuteron, suggested by Hulthén, gives the normalized momentum distribution,[7]

$$H(p)=\frac{4}{\pi}\left[\frac{\alpha\beta(\alpha+\beta)}{(\alpha-\beta)^2}\right]\left(\frac{1}{\alpha^2+p^2}-\frac{1}{\beta^2+p^2}\right)^2 p^2, \qquad (1)$$

where $\alpha=(mE)^{1/2}=45.5$ MeV/c, with m equal to the

[5] J. Peter Berge, Frank T. Solmitz, and Horace D. Taft, University of California Lawrence Radiation Laboratory Report No. UCRL-9097, 1960 (unpublished).

[6] Geoffrey F. Chew, Phys. Rev. **80**, 196 (1950).

[7] L. Hulthén, Arkiv Mat. Astron. Fysik **35A**, No. 25 (1948).

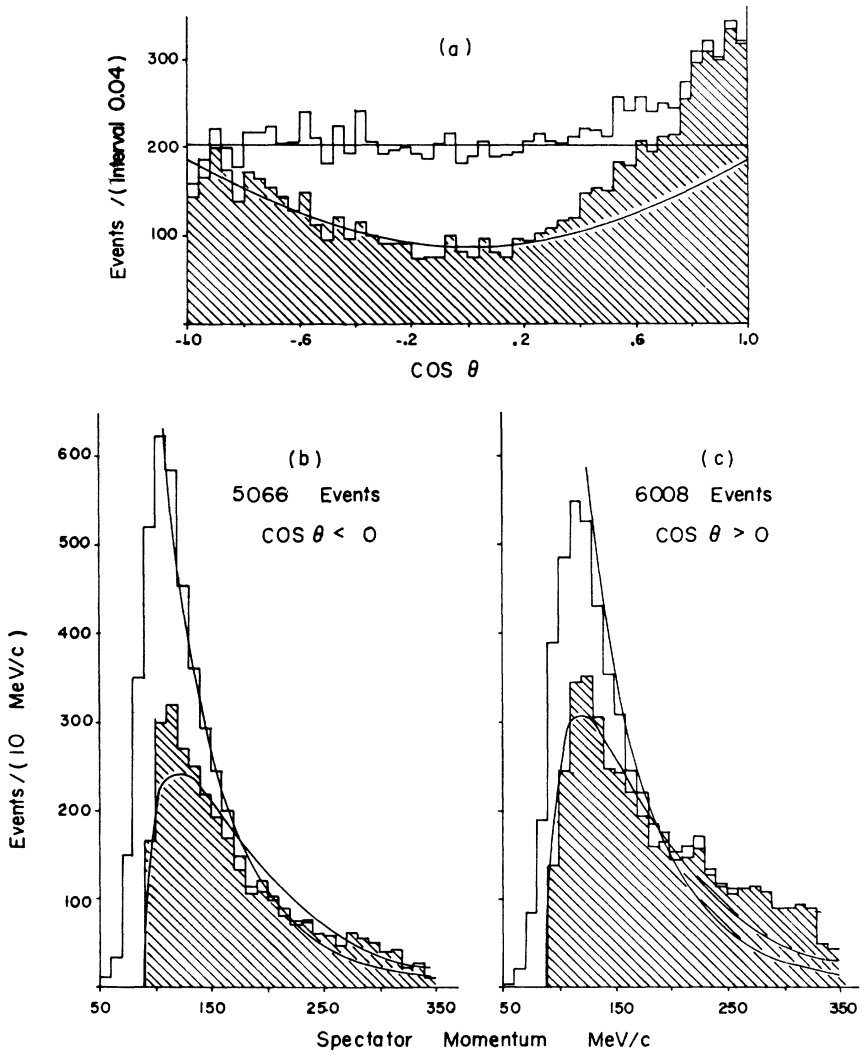

FIG. 1. Spectator proton distributions: (a) cosine of angle between spectator and beam, (b) momentum of backward spectators, and (c) momentum of forward spectators. Shaded events have projected momentum greater than 90 MeV/c in the scanning plane. The curves are the prediction of the Hulthén wave function.

nucleon mass and E equal to the deuteron binding energy. β is a parameter which is chosen to be 5.2α.

The angular distribution associated with the Hulthén wave function is isotropic.

The distributions of the magnitude and direction of the spectator protons from the four-prong events are shown in Fig. 1. An event in the $p\pi^+\pi^+\pi^-n$ final state was added to these histograms only if the momentum of the proton was less than that of the neutron. The final state $p\pi^+\pi^+\pi^-$MM was excluded since it was impossible to make a consistent separation of spectator proton and spectator neutron events in that sample. The angle θ in Fig. 1(a) is the laboratory angle between the spectator and the beam (forward) direction.

The shaded histograms include only events which have a projected momentum in the xy plane of greater than 90 MeV/c (approximately 1.5 mm on the scanning table). This cut was an attempt to eliminate the scanning and measuring biases associated with very short tracks and to predict the three-prong four-prong separation in a reasonable way. The curves are the predictions of the Hulthén function, normalized to the data between 125 and 235 MeV/c for the solid histograms and between 95 and 235 MeV/c for the shaded ones. The angular distributions were normalized to the backward hemisphere.

In order to examine some of the effects influencing the momentum distribution, the sample was divided. Spectator protons in the backward hemisphere ($\cos\theta<0$) are shown in Fig. 1(b); forward spectators are shown in Fig. 1(c).[8] The impulse model describes the backward hemisphere quite well. However, in the forward direction there are too many high-momentum and too few low-momentum spectators relative to the prediction. Also, the hemispheres are not equally populated.

It is not necessary to place all of the blame for these discrepancies on the impulse model. There are several effects which may contribute to an explanation. For example, it is likely that there are some interactions

[8] This division was made at the suggestion of Dr. Robert Eisner.

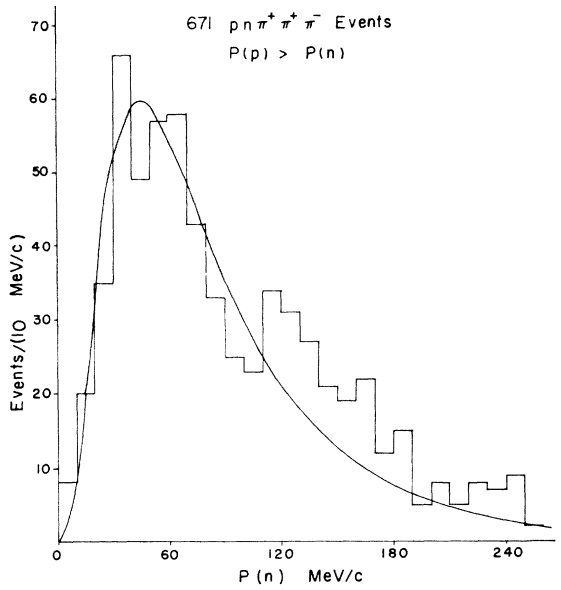

FIG. 2. Spectator-neutron momentum distribution. The curve is the impulse model prediction.

between the spectator and the other particles in the final state. This may explain why the impulse model describes the backward spectators so much better than the forward ones. The rest of the final-state particles are almost always forward in the laboratory and therefore it is less likely that they would interact with a backward spectator than with one also going forward. This effect would distort the momentum and angular distributions in the observed way; the "spectator" would pick up additional momentum in the beam direction. Final-state spectator interactions might also be expected to increase with the multiplicity of the final state. In fact, the excess of forward spectators seen in Fig. 1 comes predominantly from the $pp\pi^+\pi^-$MM final state. In the final state $pp\pi^+\pi^-$, on the other hand, there are more spectator protons in the backward hemisphere than in the forward.

While the final-state spectator interactions are not a violation of the impulse model in the sense that the original interaction involves only one nucleon of the deuteron, it does reduce the utility of the model. The information about the original interaction is obscured.

Another effect which must be considered is the energy dependence of the interaction cross section. Forward spectators imply a center-of-mass energy, for the system exclusive of the spectator, higher than that of the backward-spectator events. For a beam momentum of 2.7 GeV/c the range of this energy in the impulse model is from about 2.1 to 2.7 GeV. It is not unlikely that cross sections for certain final states vary by a factor of 2 or 3 over this interval.[9] The excess of events with backward spectators in the $pp\pi^+\pi^-$ final state, for example, is in agreement with the falling cross section for that channel.

Finally, there is probably an additional scanning bias in the forward hemisphere because of the three other forward tracks, which may obscure the spectator track. [This effect can also be seen in the extreme backward direction, $\cos\theta \approx -1$, in Fig. 1(a), where the spectator track lies on top of the beam track.] While this bias may contribute to a deficiency of low-momentum forward spectators, it is contrary to the over-all excess of spectators in the forward hemisphere. Nevertheless, it is interesting to look at a spectator momentum distribution that is free from scanning biases, Fig. 2. These are the neutrons in the final state $p\pi^+\pi^+\pi^-n$ which have a lower momentum than the proton.

In conclusion, the impulse approximation is at least as good as the agreement between the data and the predictions in Figs. 1 and 2. Energy dependent cross sections and final-state interactions of the spectator probably both contribute to the deviation of the spectator distributions from the model. Even in the cases where a final-state interaction occurs, the model still has some validity although the approximation is less exact. The reader should be aware of these limitations whenever the interaction is referred to as π^+n.

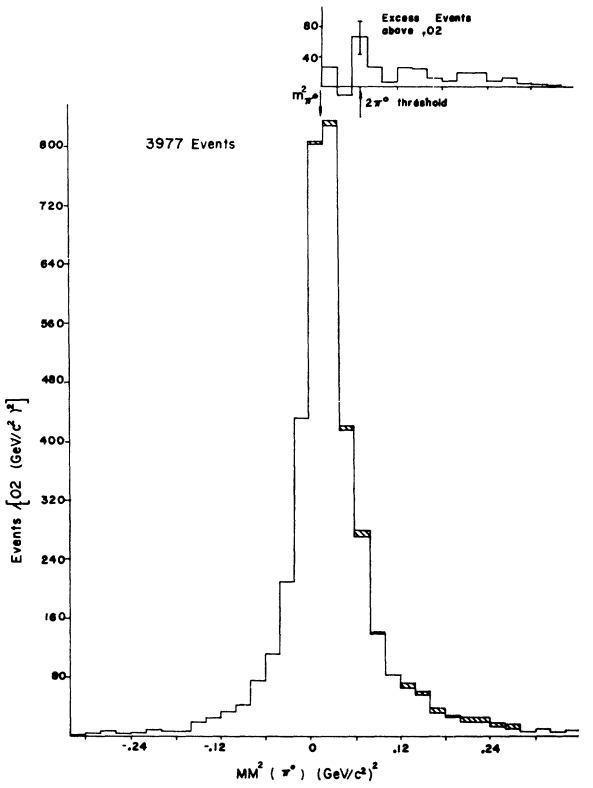

FIG. 3. Unfitted π^0 mass squared from the $pp\pi^+\pi^-\pi^0$ final state. Shaded events are ambiguous with other one-constraint fits. The insert is the difference between the number of events to the right and the left of 0.02 (GeV/c^2)^2.

[9] See Fig. 23.

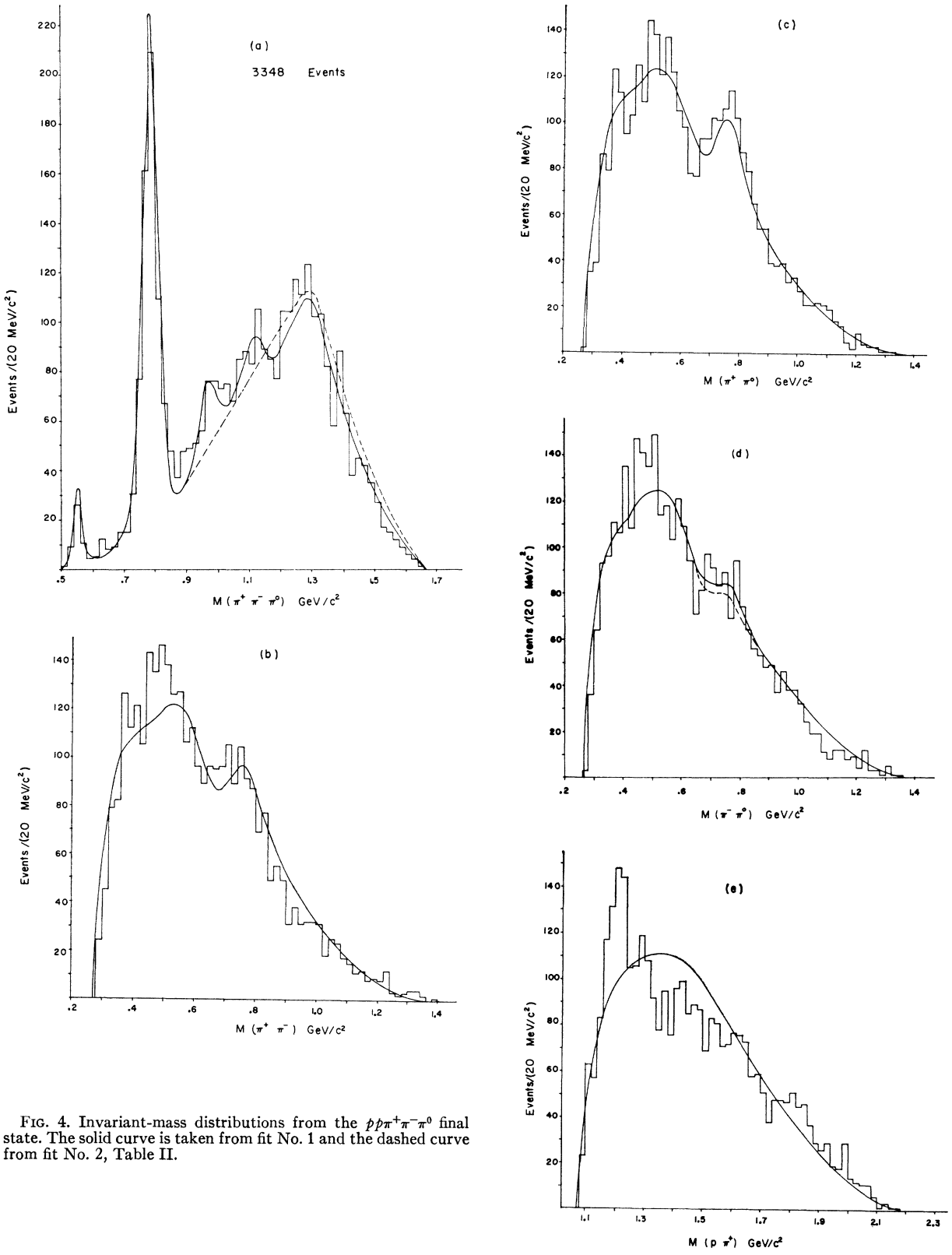

FIG. 4. Invariant-mass distributions from the $pp\pi^+\pi^-\pi^0$ final state. The solid curve is taken from fit No. 1 and the dashed curve from fit No. 2, Table II.

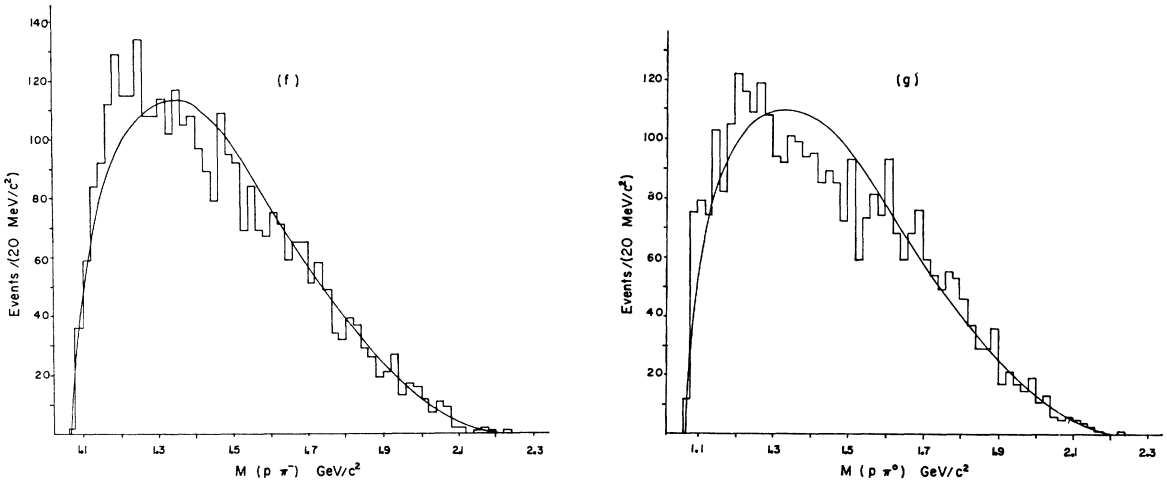

FIG. 4. (*continued*).

Some of the conventions involved in the application of the impulse model are described in the Appendix.

V. FINAL STATE $pp\pi^+\pi^-\pi^0$

A. Tests of Sample Purity

The mass squared of the unfitted neutral calculated from the $pp\pi^+\pi^-\pi^0$ sample is shown in Fig. 3. The shading shows the contribution of events which are ambiguous with other one-constraint fits.

The sample was examined for contamination from several sources. Approximately 100 of these events also fit the $pp\pi^+\pi^-$ hypothesis with a confidence level less than 0.01. These had a MM^2 distribution nearly symmetric about zero, and showed no evidence of an ω peak in the $M(\pi^+\pi^-\pi^0)$ spectrum contrary to the remainder of the π^0 events. Since the number of these events was also consistent with that expected in the tail of the $pp\pi^+\pi^-$ χ^2 distribution, these events were excluded from the π^0 sample.

Evidence for contamination from the final state ppK^+K^- was also seen in events fitted by a low momentum π^0. The square of the mass of the final-state meson could be calculated[10] and the suspected K^+K^- events were removed from the final π^0 sample.

The measurement resolution was not sufficient to permit a separation of missing γ's from missing π^0's. However, any sizable fraction of γ events would certainly distort the π^0 missing mass spectrum on the low side. No evidence of this is apparent in Fig. 3.

It was also impossible to completely eliminate events having two π^0's. One method used to estimate the amount of this contamination was to look at the asymmetry of the π^0 peak, shown in the insert of Fig. 3. The difference between the bins equidistant from 0.02 $(\text{GeV}/c^2)^2$ was plotted and the excess on the high-mass side amounts to about 200 events. However, this is probably an over estimate of the $2\pi^0$ contamination. A Monte Carlo calculation using $2\pi^0$ phase space with typical measuring errors predicted that no more than about 50 of the $2\pi^0$ events would fit the single π^0 hypothesis.

B. Invariant-Mass Distributions

The invariant mass of several of the particle combinations from the $pp\pi^+\pi^-\pi^0$ final state are shown in Fig. 4. The proton referred to in plots (e), (f), and (g) is the assumed nonspectator (higher-momentum) proton. In the $M(\pi^+\pi^-\pi^0)$ spectrum signals for the η and ω mesons are obvious. The structure above 0.9 GeV/c^2 is not so clear but suggestions of peaks can be seen at masses 1.0, 1.1, and 1.3 GeV/c^2 which may be associated with the H, A_1, and A_2 mesons.[11] The $M(2\pi)$ spectra all show evidence for ρ production, especially in the positive-charge state, Fig. 4(c).

A variety of fits to these distributions were attempted using the maximum-likelihood fitting program MURTLEBERT,[12] obtained from the High Energy Physics Group at Berkeley. The mass, widths, and amounts of Gaussian and Breit-Wigner resonance functions were used as parameters. Since several of the mass distributions were fitted simultaneously, resonance reflections and cascade decay processes of the type $A \to \rho\pi \to \pi\pi\pi$ could be handled in a reasonable way. The smearing of the center-of-mass energy according to a spectator model of the interaction was also included.

[10] See Ref. 1, p. 30; also, R. Ehrlich, R. J. Plano, and J. B. Whittaker, Phys. Rev. Letters **20**, 686 (1968).

[11] A recent explanation of the H enhancement suggests that it is a kinematic result of ρ band cuts. S. Fung, W. Jackson, R. T. Pu, D. Brown, and G. Gidal, Phys. Rev. Letters **21**, 47 (1968). In our data, however, whatever indication that exists for a bump around 1.0 GeV/c^2 is as strong in the $M(3\pi)$ distribution, Fig. 4(a), as it is in the distributions with ρ cuts, Fig. 9. There are expected to be 15–20 events in this region from $\eta' \to \pi^+\pi^-\gamma$.

[12] Jerry Friedman, University of California Lawrence Radiation Laboratory, Alvarez Programming Group Note No. P-156, 1966 (unpublished).

Two sets of typical results are given in Table II and drawn onto Fig. 4. For these fits only the fractional amounts of the processes were parameters; the masses and widths of the resonances were fixed at the values indicated in parentheses. Breit-Wigner functions were used for all the resonances except for the η and ω, where the Gaussian form was used. The solid curves in Fig. 4 represent a Monte Carlo sample generated using the results of fit No. 1; dashed curves show the result when the H and A_1 processes are not included, fit No. 2.

Adding the two extra 3π resonances obviously improves the representation of the data, not only in the resonance region but also on the upper edge of the 3π mass spectrum. However, there are several approximations in these fits which make any conclusions about the existence of the H or A_1 on this basis alone somewhat questionable. In the first place, phase space is not an adequate description of the background. The π's are known to be produced peripherally, independent of resonance effects. This is accompanied by a shift of the background peaks in the mass spectra of the π's to lower values than the phase-space peaks. Also, Deck processes involving peripheral ρ production with diffractive scattering of the other π [Fig. 9(b)] were not included.[13] Finally, the production and decay angular distributions of the resonances were not taken into account. Some of these effects undoubtedly contribute to the relatively poorer description of the $M(p\pi)$ distributions by the fitting procedure.

TABLE II. Processes contributing to the $pp\pi^+\pi^-\pi^0$ final state.

Process	Fraction of $p\pi^+\pi^-\pi^0$ final state fit No. 1	fit No. 2
$\pi^+n \to p\eta(548,31)$ $\searrow$ $\pi^+\pi^-\pi^0$	0.012±0.002	0.012±0.002
$\pi^+n \to p\omega(783,59)$ $\searrow$ $\pi^+\pi^-\pi^0$	0.170±0.007	0.167±0.007
$\pi^+n \to pH(960,80)$ $\searrow$ $\pi^+\pi^-\pi^0$	0.041±0.009	···
$\pi^+n \to pA_1(1105,80)$ $\searrow$ $\rho^\pm\pi^\pm$ $\searrow$ $\pi^\pm\pi^0$	0.025±0.009	···
$\pi^+n \to pA_2(1295,140)$ $\searrow$ $\rho^\pm\pi^\mp$ $\searrow$ $\pi^\pm\pi^0$	0.067±0.014	0.043±0.012
$\pi^+n \to p\pi^0\rho^0(1770,140)$[a] $\searrow$ $\pi^+\pi^-$	0.080±0.013	0.099±0.012
$\pi^+n \to p\pi^-\rho^+(770,140)$[a] $\searrow$ $\pi^+\pi^0$	0.080±0.013	0.099±0.012
$\pi^+n \to p\pi^+\pi^-\pi^0$(phase space)	0.525	0.580
χ^2/degrees of freedom	357/230	426/232

[a] Constrained to be equal. (See Ref. 35.)

[13] R. J. Deck, Phys. Rev. Letters **12**, 340 (1964).

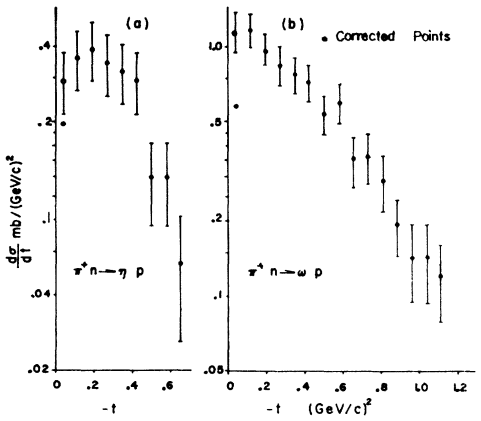

FIG. 5. Differential cross sections for η and ω production. The corrections are from Fig. 6.

C. Mass Resolution

The widths of the η and ω were assumed to represent good estimates of the experimental $M(3\pi)$ resolution. The mass dependence of this resolution was estimated by forming the function

$$f(x)=\sum_i \frac{1}{\sigma_i} e^{-x^2/\sigma_i^2} \qquad (2)$$

with the summation over events within a restricted range in $M(3\pi)$. σ_i was the uncertainty in $M(3\pi)$ calculated from the fitted momenta. The σ_i were scaled so that the width of $f(x)$ was consistent with the width of the η and ω peaks. With this definition the full width at half-maximum of $f(x)$ varied from about 30 MeV/c^2 at $M(3\pi)=0.5$ MeV/c to about 70 MeV/c^2 at $M(3\pi)=1.5$ GeV/c^2.

D. η Meson

The mass and width of the η have been fitted at 548±3 and 31±5 MeV/c^2, respectively.[14]

The differential cross section for η production is shown in Fig. 5(a). The plot includes 66 $\eta \to \pi^+\pi^-\pi^0$ and 182 $\eta \to$ neutral, although this latter sample contains substantial $2\pi^0$ background.[1,15] The cross section is scaled from the $\pi^+\pi^-\pi^0$ events to include all decay modes.[16]

E. Corrections to Differential Cross Section

Several corrections have been made to the differential cross sections in the forward direction. The width of the

[14] All widths quoted here will refer to the full width at half-maximum.

[15] J. Gezelter, S. Lichtman, F. J. Loeffler, R. J. Miller, and R. B. Willmann, Nuovo Cimento **53**, 213 (1968).

[16] C. Baltay, P. Franzini, J. Kim, L. Kirsch, R. Newman, N. Yeh, J. Cole, J. Lee-Franzini, and H. Yarger, Phys. Rev. Letters **19**, 1498 (1967).

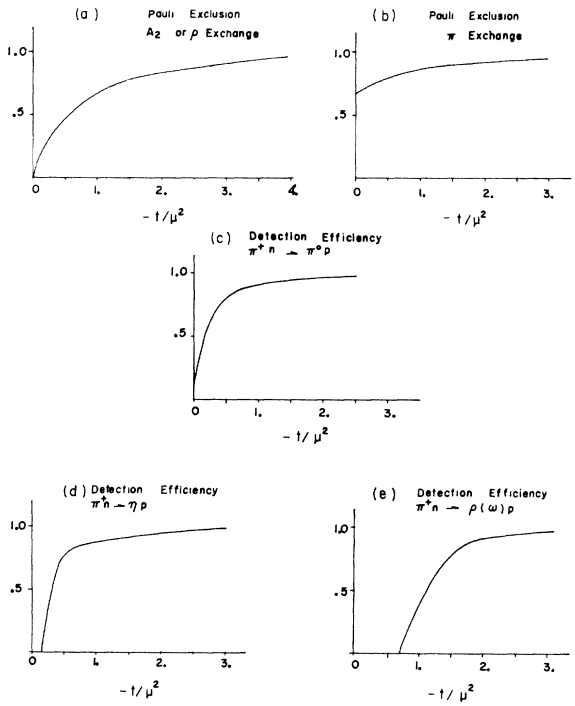

FIG. 6. Corrections to the differential cross sections. See text for explanation.

first bin is somewhat smaller than the others due to the nonzero kinematic lower limit on t. The number of events in this bin has been adjusted to bring the cross section into scale with the rest of the plot.

There is expected to be some scanning bias against events having very small momentum transfers. An estimate of this effect has been made by assuming that the Hulthén wave function describes the initial momentum distribution of the interaction nucleon and that only events in which the nonspectator nucleon had a final-state momentum greater than 100 MeV/c would be included in the four-prong sample. The resulting detection efficiency as a function of momentum transfer is shown in Figs. 6(c)–6(e) for the production of mesons of several different masses.

A correction has also been made for the restriction on the spin-nonflip amplitude required by the exclusion principle for two very low momentum protons.[17] Since the isospin of one nucleon flips, if the spatial wave function of the two-nucleon system is not disturbed, the spin of the nucleon must also flip to satisfy the symmetry requirements. The curves of Figs. 6(a) and 6(b) are taken from the tabulation of Benson[18] and involve a calculation by Phillips and Rarita[19] for the spin-flip and spin-nonflip contributions to the amplitude based on an exchange model.

F. ω Meson

The mass of the ω has been determined to be 784 ± 2 MeV/c^2 and the experimental width is 59 ± 5 MeV/c^2 from a fit to a Gaussian in mass squared.

Figure 5(b) shows the differential production cross section of the ω. Again the data have been scaled to include all decay modes and are corrected in the forward direction by the factors of Figs. 6(a) and 6(e). As in other experiments,[18,20] there is no dip at $t=-0.6$ (GeV/c)^2, contrary to the prediction of the Regge-pole model with a simple ρ trajectory exchange.[21]

The angular distributions of the ω decay are shown in Fig. 7. In the reference frame defied in Fig. 7(a), the angular distribution for a $J=1$ particle decaying into

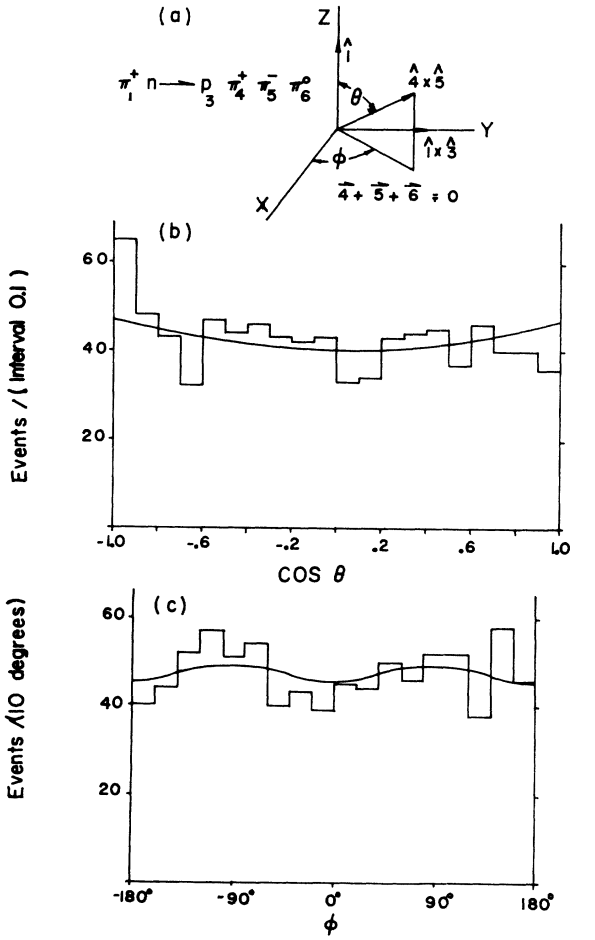

FIG. 7. Angular distributions of ω decay: (a) definition of the decay angles, (b) cosθ, and (c) ϕ. The curves in (b) and (c) are Eq. (4) with the average values of $\rho_{00}(0.37\pm0.02)$ and $\rho_{1-1}(0.02\pm0.02)$.

[17] I. Butterworth, J. Brown, G. Goldhaber, S. Goldhaber, A. Hirata, J. Kadyk, B. Schwarzschild, and G. Trilling, Phys. Rev. Letters **15**, 734 (1965).

[18] G. Benson, University of Michigan Technical Report No. COO-1112-4, 1966 (unpublished).

[19] R. J. Phillips and W. Rarita, Phys. Rev. **139**, B1336 (1965).

[20] H. O. Cohn, W. M. Bugg, and G. T. Condo, Phys. Letters **15**, 344 (1965).

[21] Ling-Lie Wang, Phys. Rev. Letters **16**, 756 (1966).

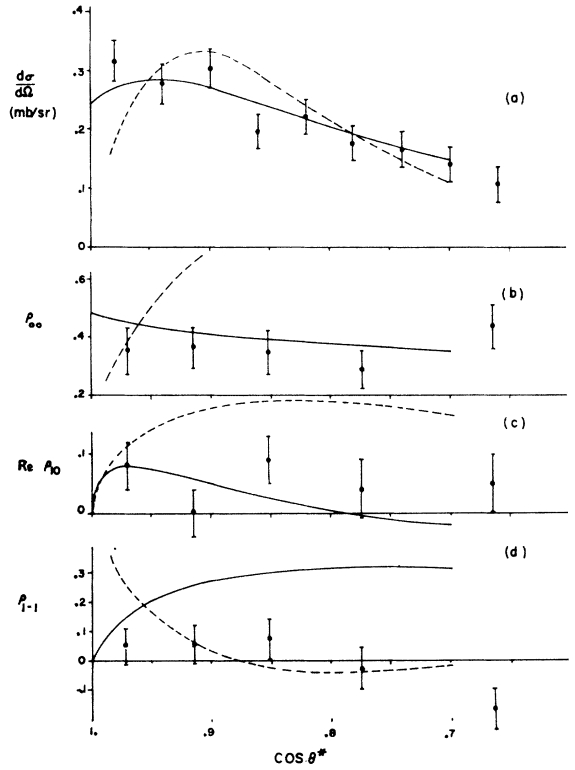

FIG. 8. Details of ω production in the forward direction. The solid curves are the prediction of a ρ-exchange model with absorption (Refs. 24–27). The dashed curves follow from a Regge-pole model with ρ and B trajectories exchanged (Ref. 23).

three pseudoscalar mesons is[22]

$$W(\theta,\phi)=(3/8\pi)[(1-\rho_{00})+(3\rho_{00}-1)\cos^2\theta - 2\rho_{1-1}\sin^2\theta\cos 2\phi - 2\sqrt{2}\,\mathrm{Re}\rho_{10}\sin 2\theta\cos\phi], \quad (3)$$

where the $\rho_{mm'}$ are the density matrix elements describing the spin states of the ω. Integrating the distribution over either of the angles gives

$$W(\theta)=\tfrac{3}{4}[(1-\rho_{00})+(3\rho_{00}-1)\cos^2\theta], \qquad W(\phi)=(1/2\pi)[1-2\rho_{1-1}\cos 2\phi]. \quad (4)$$

The density matrix elements involved in Eq. (3) have been determined for several regions of the center-of-mass production angle of the ω by a maximum-likelihood fit to the data. The curves in Fig. 7 were computed [Eq. (4)] with the average values of ρ_{00} and ρ_{1-1}, 0.37 ± 0.02 and 0.02 ± 0.02, respectively.

Details of the ω production in the forward direction are shown in Fig. 8. The error bars indicate statistical uncertainty. The dashed curves are the result of a Regge-pole model as calculated by Barmawi for the $\pi^+n\to\omega p$ reaction at 3.2 GeV/c π^+ laboratory momentum.[23] The theory includes the exchange of ρ and B trajectories. The predicted differential cross section has been scaled by a factor 1.3 to give the best fit to this data.

The set of solid curves are the prediction of a ρ-exchange model with absorption effects included.[24–27] The values of the parameters (notation of Ref. 26) which describe the initial-state absorption were fixed at

$$C_1=\sigma_T/(4\pi A)=0.87, \quad \gamma_1=1/(2q^2A)=0.054,$$

where σ_T is the total π^-p cross section at this energy[28] (32 mb corresponds to 82 GeV^{-2}), A is the exponential slope of the π^-p elastic differential cross section[29] $d\sigma/dt\propto e^{-AT}$ ($A=7.8$ GeV^{-2}), and q is the center-of-mass momentum of either particle in the initial state. The final-state absorption parameters were fixed at the values suggested in Ref. 26,

$$C_2=1.0, \quad \gamma_2=3\gamma_1/4=0.041.$$

Two variable parameters were used:

$$G_{\rho np}{}^T/G_{\rho np}{}^V=2.2,$$

which was varied to fit the shape of $d\sigma/d\Omega$ and

$$(f_{\pi\rho\omega}{}^2/4\pi)[(G_{\rho np}{}^V)^2/4\pi]=9.6,$$

which was varied to fit the magnitude of $d\sigma/d\Omega$.

To the extent that the coupling constants in these last two relations can be extracted from an essentially phenomenological model, it is interesting to compare these values with ones determined by other means.

Vector dominance predicts[24] the ratio G^T/G^V to be $\mu_p-\mu_n-1=3.7$, where μ is the magnetic moment of the nucleon. The value determined by Scotti and Wong[30] from nucleon-nucleon scattering data is 3.0.

Using the value of 1.2 for $(G^V)^2/4\pi$, consistent with the value quoted by Scotti and Wong and with that determined from S-wave πN scattering,[24] gives $f_{\pi\rho\omega}{}^2/4\pi=8.0$ compared to $f^2/4\pi\approx 4g_{\pi\pi\rho}{}^2/4\pi=9.8$, from the strong interaction sum rule,[31] and $f^2/4\pi=15$ from the virtual ρ model of $\omega\to\pi^+\pi^-\pi^0$ decay or from a vector dominance model of the decay $\pi^0\to 2\gamma$ or $\omega\to\pi^0\gamma$.[32,33]

[22] J. D. Jackson, J. T. Donahue, K. Gottfried, R. Keyser, and B. E. Y. Svensson, Phys. Rev. **139**, B428 (1965).
[23] M. Barmawi, Phys. Rev. **166**, 1857 (1968).
[24] J. D. Jackson and H. Pilkuhn, Nuovo Cimento **33**, 906 (1964).
[25] K. Gottfried and J. D. Jackson, Nuovo Cimento **33**, 309 (1964).
[26] J. D. Jackson, Rev. Mod. Phys. **37**, 484 (1965).
[27] R. Keyser, CERN Memo 66/438/5/p/he, 1966 (unpublished).
[28] A. Citron, W. Galbraith, T. F. Kycia, B. A. Leontic, R. H. Phillips, A. Rousset, and P. H. Sharp, Phys. Rev. **144**, 1101 (1966).
[29] D. H. Miller, L. Gutay, P. B. Johnson, F. J. Loeffler, R. L. McIlwain, R. J. Sprafka, and R. B. Willmann, Phys. Rev. **153**, 1423 (1967).
[30] A. Scotti and D. Y. Wong, Phys. Rev. **138**, B145 (1965).
[31] V. de Alfaro, S. Fubini, G. Rossetti, and G. Furlon, Phys. Letters **21**, 576 (1966).
[32] M. Gell-Mann, D. Sharp, and W. G. Wagner, Phys. Rev. Letters **8**, 261 (1962).
[33] There is a factor $M_\rho{}^2$ involved in the definition of the coupling constant in Ref. 24 relative to the definition used in Refs. 31 and 32.

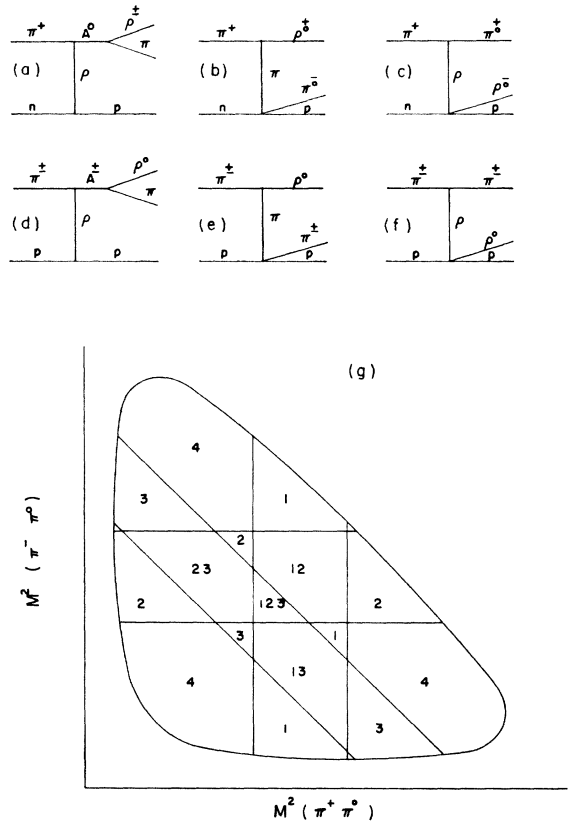

FIG. 9. Processes contributing in the region of the A mesons: (a) A production via ρ exchange, (b) ρ production via π exchange, (c) ρ production via ρ exchange, (d)–(f) similar processes from $\pi^\pm p$, and (g) ρ bands on the 3π Dalitz plot.

G. A Mesons

An examination of the neutral 3π spectrum in the region of the A mesons has several advantages over the charged 3π spectrum from $\pi^\pm p$ bubble-chamber experiments. If the A mesons are $I=1$ particles produced via an $I=1$ exchange mechanism as is usually assumed, then the cross section for the reaction $\pi^+n\to A^0p$ is twice that for the reaction $\pi^\pm p\to A^\pm p$, Figs. 9(a) and 9(d). This is easily seen by comparing the Clebsch-Gordan coefficients coupling the isospin states at the nucleon vertices. In addition, assuming that the A mesons decay predominantly via $\rho\pi$, both decay modes of the neutral A are detectable, whereas only one of the charged A modes is detectable, giving the $\pi^+\pi^-\pi^0$ system four times as many A's as $\pi^+\pi^-\pi^\pm$.

Another advantage involves the separation of the background due to the Deck effect, Figs. 9(b) and 9(e). In the $\pi^\pm p$ experiments, the A decay and the Deck effect lead to the same charge state of the ρ. In the π^+n reaction, on the other hand, all three charge states of the ρ can be detected and only ρ^+ is common to the resonance and Deck processes.

The 3π mass spectra for events having $M(2\pi)$ in a ρ band are shown in Figs. 10(a), 10(b), and 10(c), for ρ^-, ρ^+, and ρ^0, respectively. Figure 10(d) includes events in either ρ^+ or ρ^- bands. $I=1$, $\rho\pi$ resonances would be expected to show up in plots (a) and (b), but not in (c), while Deck enhancements would be expected in (b) and (c), but not (a). The shaded histograms are an attempt to enhance the first effect at the expense of the latter by selecting events which have a smaller momentum transfer (from the beam) to the 3π system than to the 2π (ρ) system.

The suggestion of separate peaks which was seen in the uncut distribution, Fig. 4(a), persists when the charged ρ-band selections are made but does not appear in the ρ^0 events.

A more quantitative examination of the A_1 and A_2 regions [$M(3\pi)=1.06$–1.18 and 1.24–1.36, respectively] was attempted in the following way.[34] Since each of the diagrams of Figs. 9(a)–9(c) populate different regions in the 3π Dalitz plot, it should be possible to estimate the contribution of each. The Dalitz plot was divided into sections, as indicated in Fig. 9(g), defined by each of the three ρ bands (0.68–0.84). The number of events in each section (N_x) was counted and the fractional area (f_x) was calculated. The number of events associated with each ρ band was then tabulated with events in overlap regions contributing with fractional weight to each band.

$$\begin{aligned} N_+&=N_1+\tfrac{1}{2}N_{12}+\tfrac{1}{2}N_{13}+\tfrac{1}{3}N_{123},\\ N_-&=N_2+\tfrac{1}{2}N_{12}+\tfrac{1}{2}N_{23}+\tfrac{1}{3}N_{123},\\ N_0&=N_3+\tfrac{1}{2}N_{13}+\tfrac{1}{2}N_{23}+\tfrac{1}{3}N_{123}. \end{aligned} \tag{5}$$

From the number of events in region 4, the non-ρ (phase-space) background in the ρ bands, N_{ps}, was estimated:

$$N_{ps}=(1-f_4)N_4/f_4. \tag{6}$$

Then, the contribution of each of the diagrams in Figs.

TABLE III. Processes contributing in the region of the A mesons.

	$A_1(1.06$–$1.18)$	$A_2(1.24$–$1.36)$
N_{total}	627	717
N_+ (ρ^+ band)	181	192
N_- (ρ^- band)	142	162
N_0 (ρ^0 band)	142	168
N_4 (non-ρ)	162	195
N_a (A via ρ exchange)	90	66
N_b (ρ via π exchange)	88	78
N_c (ρ via ρ exchange)	12	18
f_a	0.15	0.10
f_b	0.15	0.10
f_c	0	0.0
f_{ps}	0.70	0.80

[34] There is no evidence in this data for the splitting of the A_2. It has been treated as a single object for the purpose of this analysis. Actually, the lower half of the A_2 region is predominant in this experiment; the upper limit on $M(3\pi)$ is between 1.3 and 1.65 GeV/c^2 depending on the momentum of the spectator proton.

9(a)–9(c) is noted[35]:

$$N_+=\tfrac{1}{2}N_a+\tfrac{1}{2}N_b+\tfrac{1}{3}N_{\rm ps},$$
$$N_-=\tfrac{1}{2}N_a+\tfrac{1}{2}N_c+\tfrac{1}{3}N_{\rm ps}, \quad (7)$$
$$N_0=\tfrac{1}{2}N_b+\tfrac{1}{2}N_c+\tfrac{1}{3}N_{\rm ps}.$$

The number of events associated with each process is, therefore,

$$N_a=N_++N_--N_0-\tfrac{1}{3}N_{\rm ps},$$
$$N_b=N_++N_0-N_--\tfrac{1}{3}N_{\rm ps}, \quad (8)$$
$$N_c=N_-+N_0-N_+-\tfrac{1}{3}N_{\rm ps}.$$

The results are shown in Table III; the f's refer to the fractional amounts of the events in the A regions associated with each process. Assuming, then, that the diagrams of Figs. 9(a)–9(c) contribute in this proportion, an attempt was made to determine the spin and parity of the resonating $\rho\pi$ system. The expected density of points on the 3π Dalitz plot was calculated for several values of the total and orbital angular momentum,

$$D^{Jl}=f_aD_a{}^{Jl}+f_bD_b+f_cD_c+f_{\rm ps}D_{\rm ps}. \quad (9)$$

The D_i are the density functions associated with each of the processes of Fig. 9 plus phase space. They are functions of the invariant Dalitz-plot variables $M^2(\pi^+\pi^0)$, $M^2(\pi^-\pi^0)$, and $M^2(\pi^+\pi^-\pi^0)$ with symmetry properties appropriate to the decay of a meson of spin J and parity $(-1)^l$.

The description of the A decay which was used is essentially that of Frazer, Fulco, and Halpern[36] and includes the effects of the interference between the A decay modes. No other interference between diagrams was assumed. The $\rho\pi$ systems of processes (b) and (c) were assumed to have $l=0$.

The D^{Jl} were normalized by the condition

$$\int D^{Jl}(x)dx=1, \quad (10)$$

where x denotes all of the Dalitz-plot variables. The likelihood logarithm for each of the J, l assignments was then calculated using the experimental data points x_i,

$$\ln L^{Jl}\equiv\sum_i \ln D^{Jl}(x_i). \quad (11)$$

The summation included only the events within the ρ bands on the Dalitz plot in order to minimize the effect of the non-ρ background term $D_{\rm ps}$, assumed to be phase space. The results are summarized in Table IV.

As an indication of the statistical uncertainty in this method, the expected range (expectation value of $\ln L^{Jl}$)

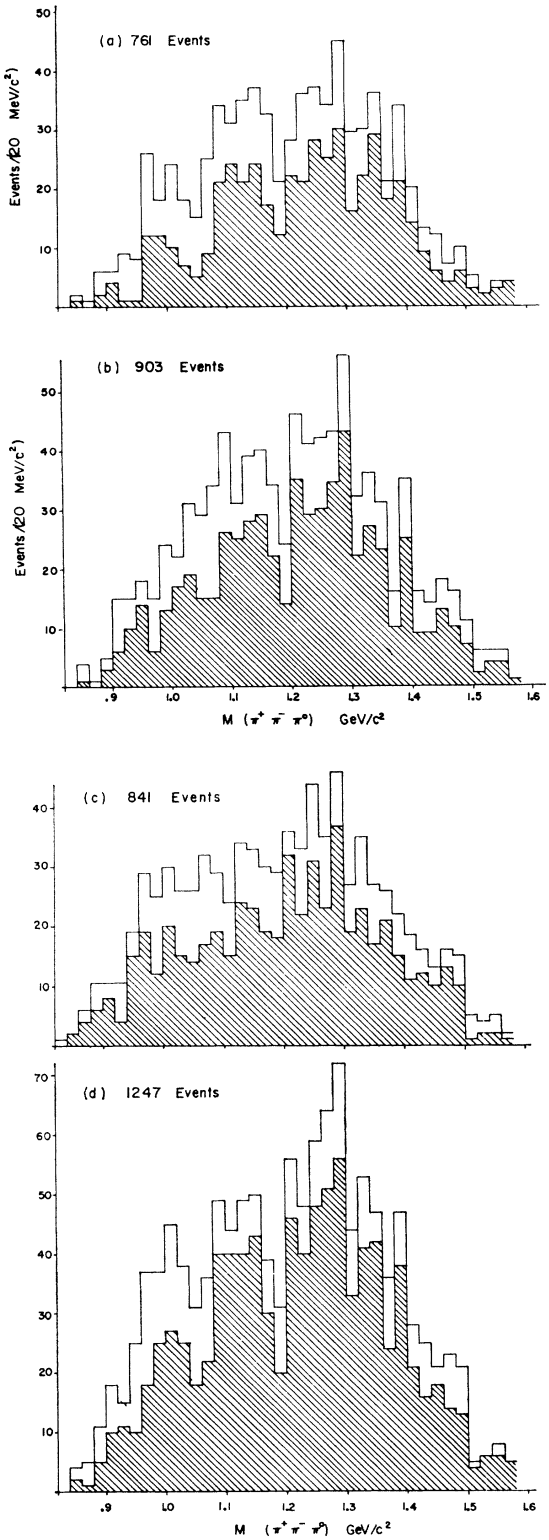

FIG. 10. $M(\pi^+\pi^-\pi^0)$ with ρ-band selection: (a) $0.66<M(\pi^-\pi^0)<0.88$, (b) $0.66<M(\pi^+\pi^0)<0.88$, (c) $0.66<M(\pi^+\pi^-)<0.88$, and (d) $0.66<[M(\pi^-\pi^0)$ or $M(\pi^+\pi^0)]<0.88$. Shaded events have smaller momentum transfer to the 3π system than to the $2\pi(\rho)$ system.

[35] The amplitudes for the two different charge configurations in Fig. 9(b) are equal since $A(\pi^0 n\to\pi^- p)=A(\pi^0 p\to\pi^+ n)=A(\pi^+ n\to\pi^0 p)$ at the lower vertex and $A(\pi^+\to\rho^+\pi^0)=A(\pi^+\to\rho^0\pi^+)$ at the upper vertex. The same consideration holds for Fig. 9(c).

[36] William R. Frazer, José R. Fulco, and Francis R. Halpern, Phys. Rev. 136, B1207 (1964).

TABLE IV. The likelihood function for various spin-parity assignments to the A mesons.

	J, l assignment					
	0, 1	1, 0	1, 1	1, 2	2, 1	2, 2
A_1:						
$\ln L^{Jl}$	466	475	462	467	474	467
$\langle \ln L^{Jl} \rangle$	(474–484)	(469–475)	(470–477)	(474–484)	(469–475)	(469–476)
L^{10}/L^{Jl}	5×10^3	1	8×10^5	5×10^3	4	5×10^3
A_2:						
$\ln L^{Jl}$	191	214	202	190	212	216
$\langle \ln L^{Jl} \rangle$	(200–209)	(200–209)	(202–212)	(202–212)	(199–207)	(205–217)
L^{22}/L^{Jl}	10^{11}	6	10^6	10^{11}	40	1

is given in parentheses. For N events the expected value of $\ln^{Jl}$ is

$$\langle \ln L^{Jl} \rangle = N \int (\ln D^{Jl}) D^{Jl} dx, \quad (12)$$

and the variance is

$$\langle \sigma^2 (\ln L^{Jl}) \rangle = N \int (\ln D^{Jl})^2 D^{Jl} dx - \langle \ln L^{Jl} \rangle^2 / N. \quad (13)$$

The ratios of the likelihood function of the best assignment to that of the others is also shown.

As an alternate approach, the functions D^{Jl} were fitted to the density of points within the ρ bands on the A_1 and A_2 Dalitz plots, taking the fractions of each process of Figs. 9(a)–9(c) plus phase space as parameters. Figure 11 shows the dependence of the χ^2 from this fit on the fraction of resonance assumed for each different spin-parity assignment. The best solution indicates $(25\pm15)\%$ A_1 with $J^p = 1^+(l=0)$ or $2^-(l=1)$, and $(15\pm10)\%$ A_2 with any of the three assignments $1^+(l=0)$, 2^+, or $2^-(l=1)$ acceptable for J^p.

Deck mechanisms and phase space alone cannot explain the data in the A_1 and A_2 regions. These processes require at least as much ρ^0 to be formed as ρ^+ and ρ^-. In fact, there are approximately equal amounts of ρ^0 and ρ^- and about 25% more ρ^+. [See Figs. 4(b)–4(d).] This ratio appears to hold in both the A_1 and A_2 regions.

H. ρ Meson

The fits to the mass distributions indicated that about 15% of the $pp\pi^+\pi^-\pi^0$ final state included ρ^0 and ρ^+ which was unassociated with either A meson. Figures 12(a)–12(c) show the $M(2\pi)$ distributions for events having small momentum transfers ($<25\ \mu^2$) from the beam to the negative, positive, and neutral 2π systems, respectively. To reduce the background, η and ω events were excluded. The neutral and positively charged combinations show evidence for approximately equal amounts of ρ but there is no evidence for ρ^-. The shaded events illustrate this difference; spectrum (a) was subtracted from (b) and (c).

The peripheral nature of the $\rho^{+,0}$ production is shown in Figs. 13(a)–13(c); the shaded events show the difference between the $\rho^{+,0}$ and ρ^- distributions. All of these features are consistent with the one-pion-exchange description of the ρ production, Fig. 9(b).

I. Δ(1238) Baryon

Assuming that the production of the $\Delta(1238)$ resonance could also be described by the π-exchange dia-

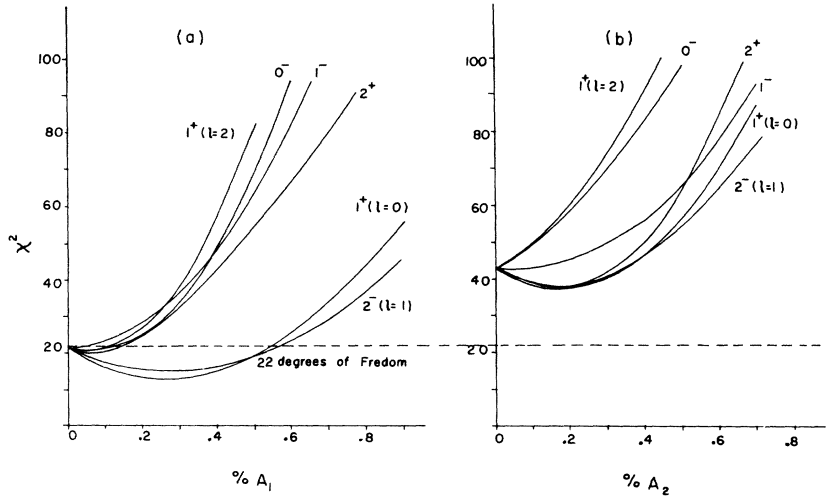

FIG. 11. Fractions of A_1 (a) and A_2 (b) predicted. The processes of Figs. 9(a)–9(c) plus phase space were fitted to the density of points in the ρ bands on the $\pi^+\pi^-\pi^0$ Dalitz plot with various spin-parity assignments for the A mesons.

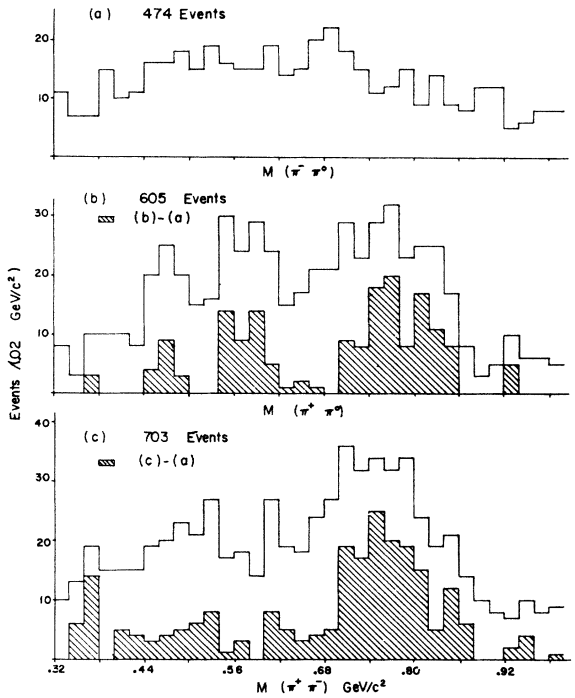

FIG. 12. $M(2\pi)$ distributions in the $pp\pi^+\pi^-\pi^0$ final state with $\Delta^2(2\pi)<25\ \mu^2$. The shaded histograms in (b) and (c) show the subtraction of spectrum (a).

gram, the amount of Δ^{++} would be expected to be small compared to the amount of Δ^0 or Δ^+. Figure 14 shows the comparison of the $M(p\pi)$ spectra for these three charge states for events with low-momentum transfer. Figures 13(d)–13(f) show the momentum-transfer distribution to events in the Δ region. The shaded histograms again show the subtraction of spectrum (d).

Although there is evidence for some peripherally produced Δ^0, it is not so easy to interpret the other charge states. There is a significant peak in the $M(p\pi^+)$ distribution, Fig. 4(e), which is hard to explain in terms of the normal exchange mechanisms of production or as reflections of other resonances. The center-of-mass production angle of the $p\pi^+$ system shows no sign of a forward peak which might be expected for baryon exchange. It is possible that this is the decay product of an s channel $N^*(2190$ or $2420)$ since the span of center-of-mass energy includes both of these values. Final-state $p\pi$ interactions may also be responsible.

VI. FINAL STATE $pp\pi^+\pi^-$

A. Tests of Sample Purity

The MM² distribution of these events is shown in Fig. 15. The sample was examined for evidence of misfitting of the reactions $\pi^+d\rightarrow ppK^+K^-$ and $pd\rightarrow ppp\pi^-$. No evidence for these reactions was found although a few cases of the latter reaction were seen and discarded during the ionization check.

TABLE V. Processes contributing to the $pp\pi^+\pi^-$ final state.

Process	Fraction of $pp\pi^+\pi^-$ final state fit No. 1	fit No. 2
$\pi^+d\rightarrow(p)p\rho(778,148)$ $\searrow\pi^+\pi^-$	0.61±0.02	0.64±0.02
$\pi^+d\rightarrow(p)pf(1250,140)$ $\searrow\pi^+\pi^-$	0.10±0.03	0.10±0.03
$\pi^+d\rightarrow(p)\pi^+\Delta^0(1238,120)$ $\searrow p\pi^-$	0.18±0.02	...
$\pi^+d\rightarrow(p)p\pi^+\pi^-$	0.11±0.03	0.26±0.03

B. Mass Distributions

The commonly studied reaction $\pi^-p\rightarrow\pi^+\pi^-n$ is less highly constrained in the kinematic reconstruction from bubble-chamber tracks than is the equivalent reaction (in the impulse approximation), $\pi^+d\rightarrow pp\pi^+\pi^-$. Consequently, the momenta and other derived variables of the latter reaction can be expected to be better resolved. However, the uncertainties inherent in the impulse model of the interaction, final-state spectator interactions, and scanning biases against low-momentum

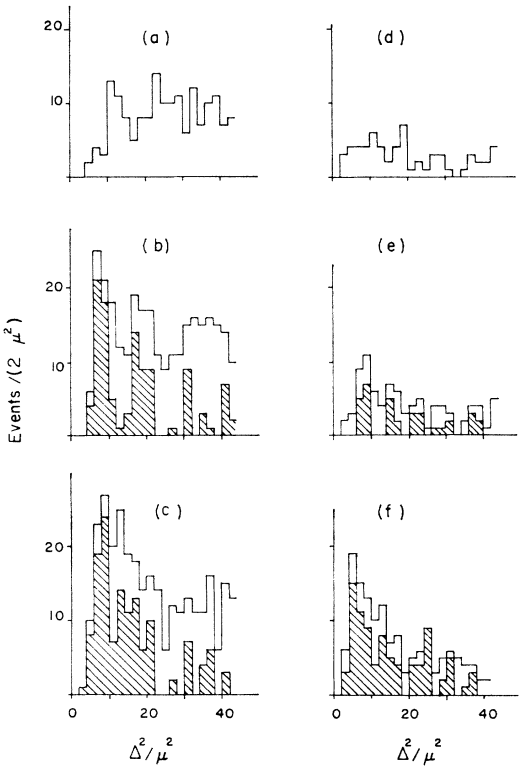

FIG. 13. Momentum-transfer distributions to 2π in the $pp\pi^+\pi^-\pi^0$ final state. $M(3\pi)>0.86$: (a) $\Delta^2(\pi^-\pi^0)$, $0.66<M(\pi^-\pi^0)<0.88$; (b) $\Delta^2(\pi^+\pi^0)$, $0.66<M(\pi^+\pi^0)<0.88$; (c) $\Delta^2(\pi^+\pi^-)$, $0.66<M(\pi^+\pi^-)<0.88$; (d) $\Delta^2(\pi^-\pi^0)$, $1.18<M(p\pi^+)<1.30$; (e) $\Delta^2(\pi^+\pi^0)$, $1.18<M(p\pi^-)<1.30$; and (f) $\Delta^2(\pi^+\pi^-)$, $1.18<M(p\pi^0)<1.30$. Shaded histograms in (b) and (c) show the subtraction of (a), and in (e) and (f), the subtraction of (d).

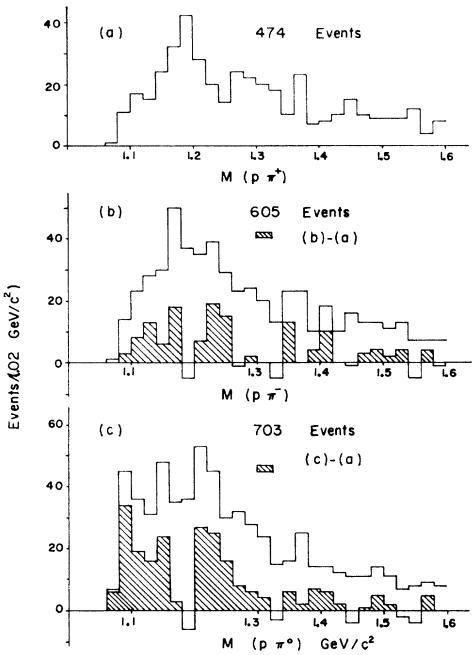

FIG. 14. $M(p\pi)$ distribution in the $pp\pi^+\pi^-\pi^0$ final state with $\Delta^2(n \to p\pi) < 25\ \mu^2$. Shaded events in (b) and (c) show the subtraction of (a).

transfer events (low-momentum protons) add to the difficulties in studying the $pp\pi^+\pi^-$ final state. For these reasons the examination of this final state from π^+d has been directed mostly toward a comparison with the isospin-symmetric state as a test of the spectator model.[37]

Both $pp\pi^+\pi^-$ and $n\pi^+\pi^-$ are dominated by the neutral ρ meson.[29,38] The extent of this contribution can be seen in the invariant-mass distributions, Fig. 16. In an attempt to simultaneously describe these three spectra, Monte Carlo samples of various resonance and phase-space processes were generated. Momentum-transfer and decay angular distributions of the ρ^0 and f^0 resonances, as determined from the experimental data, Figs. 17 and 18, were imposed on the Monte Carlo samples.

The curves in Fig. 16 and the fractions in Table V show the result of fitting the Monte Carlo distributions of $M(\pi^+\pi^-)$ and $M(p\pi^-)$ to the experimental ones. The solid curves correspond to fit No. 1 and the dashed curves to fit No. 2 [no $\Delta^0(1238)$].

A description of the $p\pi^+\pi^-$ system in terms of these processes only is not satisfactory, as Fig. 16 indicates. Including other $p\pi^-$ resonances such as $N^*(1470)$ does not give any improvement. The extreme anisotropy of the center-of-mass production angle of the 2π system, Fig. 16(d), and of the decay angles in the 2π system, Fig. 18, are strongly reflected in the $M(p\pi)$ distributions. This makes an analysis of the resonant structure of the $p\pi$ states difficult. However, there is some indication of $\Delta^{++}(1238)$ production in Fig. 16(b) which, unlike the Δ^0, cannot be described by a simple exchange model.

There is some evidence also for additional structure in the $\pi\pi$ system between the ρ and the f which has been seen in the $n\pi^+\pi^-$ final state in π^-p experiments at 4.2 and 2.7 GeV/c as well as in these data.[39] The distribution of $\cos\theta_{++}$, defined in Fig. 18(a), is strongly peaked forward and backward in this region. In an attempt to enhance this structure in the $M(\pi\pi)$ distribution, events with $\cos\theta_{++} < -0.75$ have been selected. The result is shown in the shaded histogram of Fig. 16(a).

C. ρ Meson

The mass and width of the ρ^0 meson present in this final state have been determined to be 768 ± 3 and 125 ± 10 MeV/c^2, respectively.[40] These values were obtained with the fitting program MURTLEBERT, using the mass-dependent width formulation of the Breit-Wigner

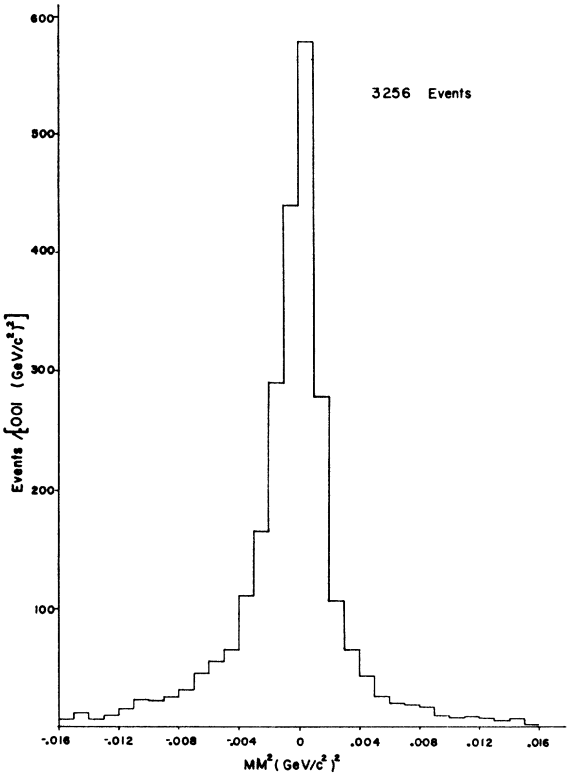

FIG. 15. Square of the missing mass from the $pp\pi^+\pi^-$ final state.

[37] See also the comparative cross sections in Sec. IX.

[38] J. P. Baton, A. Berthelot, B. Deler, O. Goussu, M. Neveu-René, A. Rogozinski, F. Shively, V. Alles-Borelli, E. Benedetti, R. Gessaroli, and P. Waloschek, Nuovo Cimento **35**, 713 (1965).

[39] D. H. Miller, L. J. Gutay, P. B. Johnson, V. P. Kenney, and Z. G. T. Guiragossian, Phys. Rev. Letters **21**, 1489 (1968); D. H. Miller, L. Gutay, S. Lichtman, F. J. Loeffler, R. J. Miller, and R. B. Willmann, Phys. Letters **28B**, 51 (1968).

[40] The resolution of $M(\pi^+\pi^-)$ in the region of the ρ, determined by the method described in Sec. V, is about 15 MeV/c^2 and has been subtracted from the maximum-likelihood solution of the ρ widths.

resonance form[41]:

$$R(m)=q_0 m_0 \Gamma_0 \frac{m}{q}\frac{\Gamma(m)}{(m_0^2-m^2)^2+[m_0\Gamma(m)]^2},$$

where

$$\Gamma(m)=\Gamma_0\left(\frac{q}{q_0}\right)^3\left[\frac{1+(q_0/r)^2}{1+(q/r)^2}\right]. \quad (14)$$

m_0 and Γ_0 are the central values of the mass and width quoted above, q is the three-momentum of either decay π in the ρ rest frame, and r is the inverse of the interaction radius, assumed to be twice the π mass.

The details of the production and decay of the ρ from this experiment are compared to the reaction $\pi^- p \to n\rho^0$ at 2.7 GeV/c[29] in Figs. 18 and 19. [For this analysis the ρ is defined by $0.66<M(\pi^+\pi^-)<0.88$.] The definition of the decay angles is given in Fig. 18(a) in a manner which preserves the expected symmetry of the two final states. The curves in Fig. 18 are of the form $A+B\cos\theta+C\cos^2\theta$, and $A+B\cos\phi$ for Figs. 18(b), 18(c), 18(d),

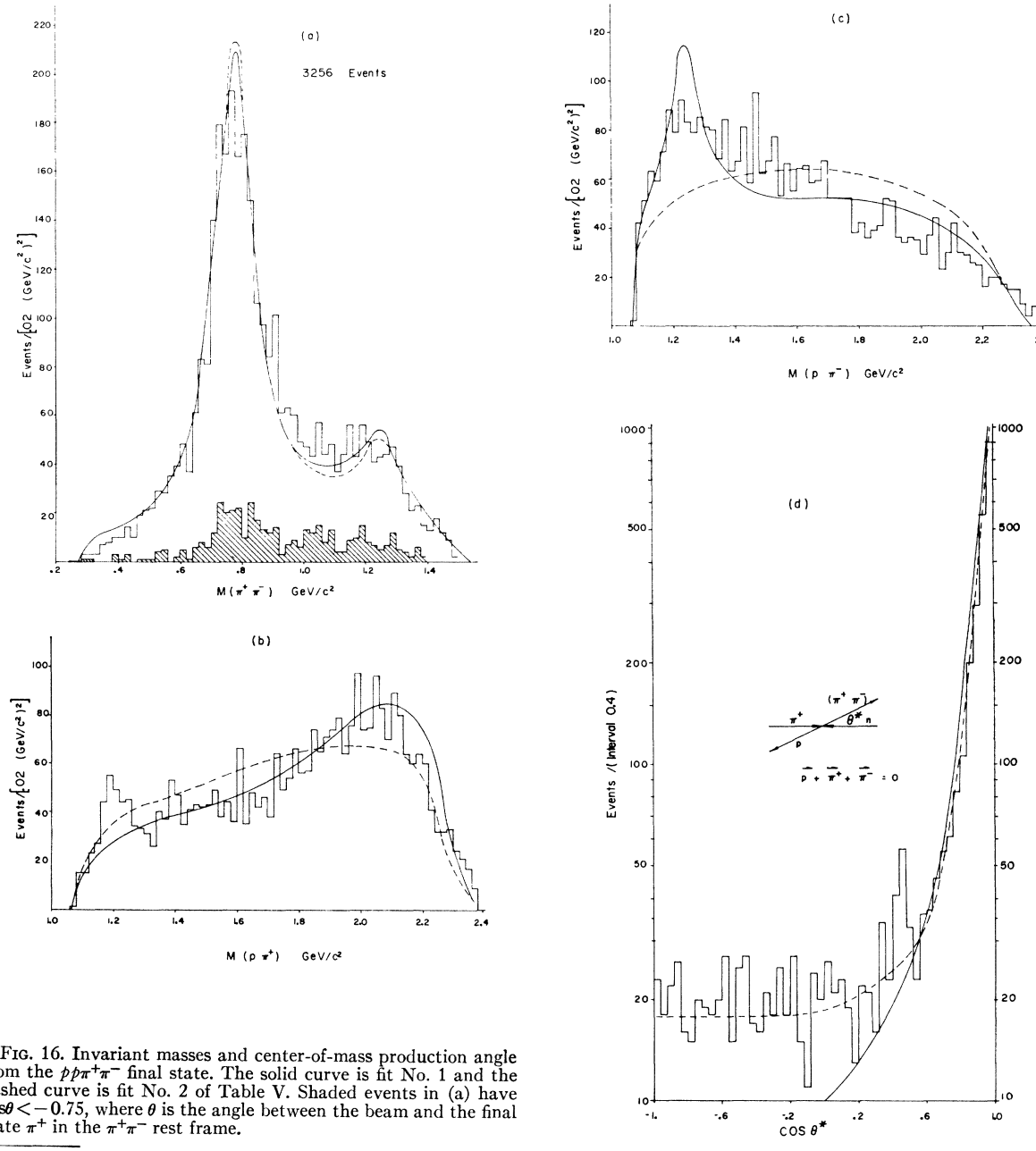

FIG. 16. Invariant masses and center-of-mass production angle from the $pp\pi^+\pi^-$ final state. The solid curve is fit No. 1 and the dashed curve is fit No. 2 of Table V. Shaded events in (a) have $\cos\theta<-0.75$, where θ is the angle between the beam and the final state π^+ in the $\pi^+\pi^-$ rest frame.

[41] J. D. Jackson, Nuovo Cimento 34, 1644 (1964).

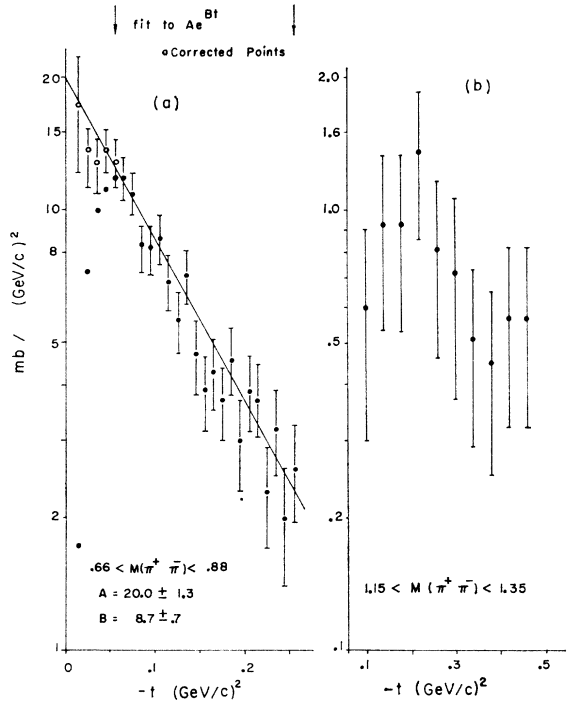

FIG. 17. Differential cross sections from the $pp\pi^+\pi^-$ final state: (a) ρ^0, (b) f^0. The corrections in (a) are from Figs. 6(b) and 6(e).

and 18(e), respectively. The coefficients were determined by fitting to the $pp\pi^+\pi^-$ data and the same curves with different normalization were drawn on the $n\pi^+\pi^-$ data. The agreement of the two different final states is quite good.

Even more dramatic is the similarity of the ρ cross section and decay distributions when compared over a range of the center-of-mass production angle. Figure 19(a) shows the differential cross section for $n\rho^0$ (triangles) and $p\rho^0$ (circles), *independently* normalized. When the corrections of Figs. 6(b) and 6(e) are made to the $p\rho^0$ final state (open circles), the agreement is excellent. The density matrix elements of the ρ^0 were determined from a fit to the distribution expected for the decay of a P-wave resonance into two pseudoscalar mesons, the same form as Eq. (3).[42] The results are shown in Figs. 19(b)–19(d). Again the $n\rho^0$ and $p\rho^0$ final states give similar results.

The curves in Fig. 19 are the prediction of the one-pion-exchange model with absorption, taken from Ref. 29.

VII. FINAL STATE $p\pi^+\pi^+\pi^-n$

A. Tests of Sample Purity

The unfitted neutron mass squared is shown in Fig. 20.[43] The shaded part of the histogram indicates the events which are ambiguous with other one-constraint hypotheses.

The first refinement of this sample was the separation of events with spectator neutrons from those with spectator protons. Since the interest was in interactions on the neutron, only events in which the proton momentum was less than that of the neutron were used. This procedure was consistent with the selection of the spectator in the final states with two protons and appears to be justified by the spectator-neutron momentum distribution, Fig. 2.

It is expected that there are very few events of the type $p\pi^+\pi^+\pi^-n\pi^0$ in this sample, since the $\pi^0 n$ threshold is at $MM^2=1.15$, relatively far out on the tail of the neutron mass peak.

B. Mass Distributions

Some of the invariant-mass distributions from the $p\pi^+\pi^+\pi^-n$ final state are shown in Fig. 21. The curves indicate the result of a MURTLEBERT fit to the processes

$$\pi^+d \rightarrow (p)n\pi^+\rho^0(770,150), \quad (23\pm3)\%$$
$$\pi^+d \rightarrow (p)\pi^+\pi^+\Delta^-(1238,150), \quad (35\pm3)\%$$
$$\pi^+d \rightarrow (p)\pi^+\pi^+\pi^-n \text{ (phase space)}, \quad (42\pm4)\%.$$

These values are in good agreement with the values determined by Alitti *et al.*[44] for the reaction

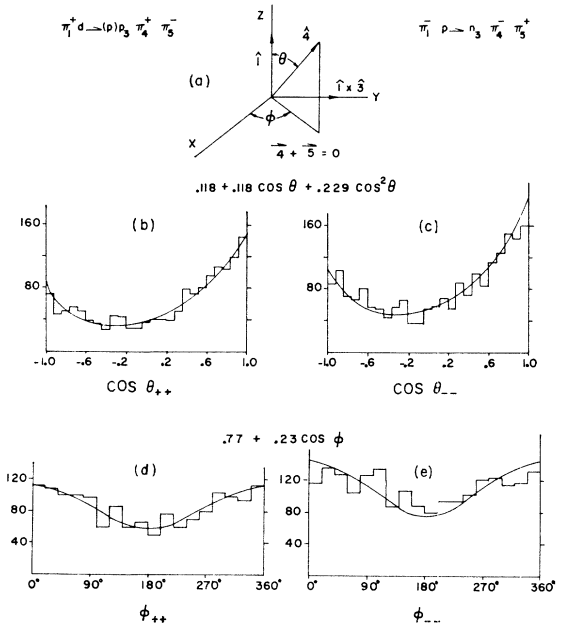

FIG. 18. Angular distributions of ρ decay: (a) definition of decay angles, (b) cosθ for $\pi^+d \rightarrow pp\rho$, (c) cos$\theta$ for $\pi^-p \rightarrow n\rho$, (d) ϕ for $\pi^+d \rightarrow pp\rho$, and (e) ϕ for $\pi^-p \rightarrow n\rho$. The curves result from fitting the data in (b) and (d). They are shown in (c) and (e) for comparison.

[42] No attempt has been made to include the effect of S-wave background in these fits.

[43] The skewing of the missing neutron mass toward the high side, an effect which is also seen in Figs. 3 and 15, is not completely understood. However, the masses calculated from the fitted momenta are not affected as evidenced by the position of the η and ω peaks.

[44] J. Alitti, J. P. Baton, A. Berthelot, B. Deler, W. J. Fickinger, N. Neveu-René, V. Alles-Borelli, R. Gessarolli, A. Romano, and P. Waloschek, Nuovo Cimento **35**, 1 (1965).

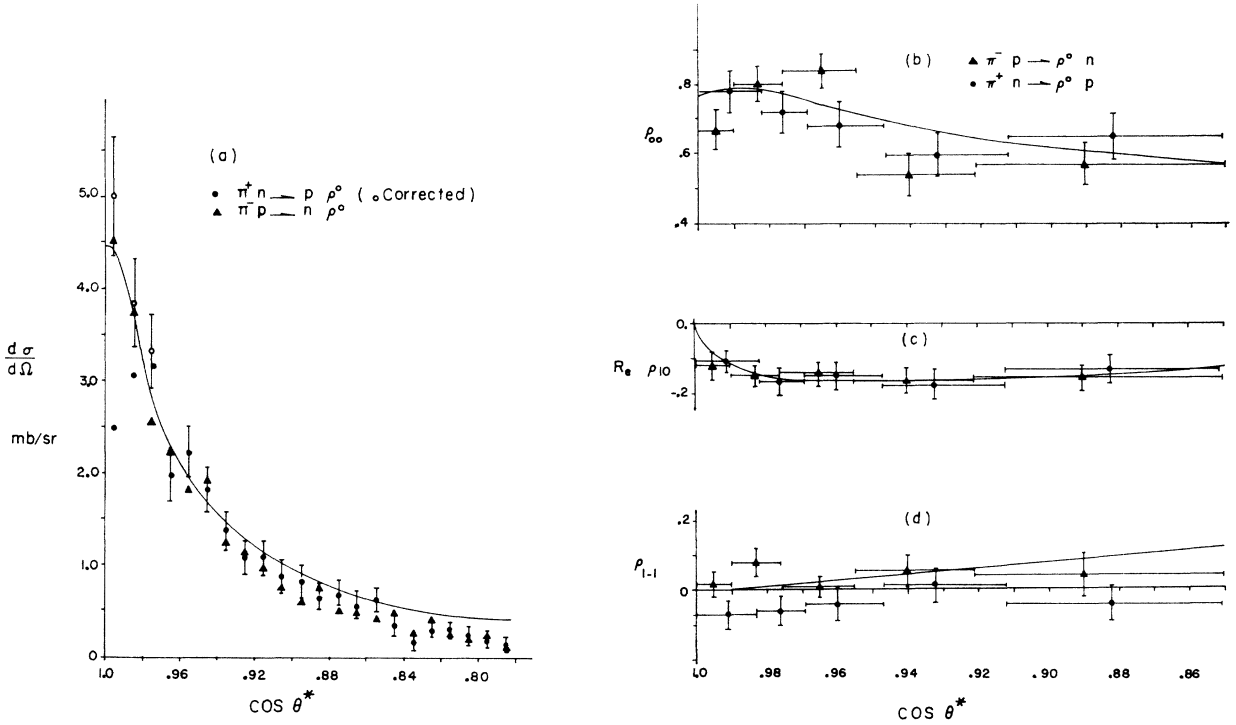

FIG. 19. Details of ρ production in the forward direction, (a) differential cross section, and (b)–(d) density matrix elements as a function of the production angle. The curves are the prediction of a pion-exchange model with absorption (Ref. 29).

$\pi^- p \rightarrow p\pi^+\pi^-\pi^-$ at 2.75 GeV/c (20% and 34% for ρ^0 and Δ^{++}, respectively). Attempts to include the process $\pi^+ d \rightarrow (p)nA_2$ and $\pi^+ d \rightarrow (p)\pi^+\pi^-\Delta^+$ in addition to the ρ^0 and Δ^- production were not satisfactory. In particular, the $n\pi^+$ spectrum is not well fitted by the simple model of phase space plus Breit-Wigner resonance shapes. From Fig. 21(a), the presence of as much as 20% Δ^+ cannot be ruled out. However, the $p\pi^0$ decay mode, Fig. 4(g), yields a smaller cross-section estimate. (See Table VII.)

The $M(\rho^0\pi^+)$ spectrum is shown shaded in Fig. 21(e). There is no clear indication of A_1 or A_2 production. However, based on the results of the analysis of the $\pi^+\pi^-\pi^0$ system, only 20–30 A_1 and A_2 events are expected in this channel, consistent with the data. This number is also consistent with the A_1 and A_2 peaks reported in the $p\pi^-\pi^-\pi^+$ final state from $\pi^- p$ experiments at this energy.[45,46]

VIII. FINAL STATES $pp\pi^+\pi^-$MM

The mass spectrum of the multiple missing neutrals from the events in the $pp\pi^+\pi^-$MM($>2\pi^0$) final states is shown in Fig. 22(a). The curve is the phase-space distribution for two missing π^0's, normalized to the area of the histogram.

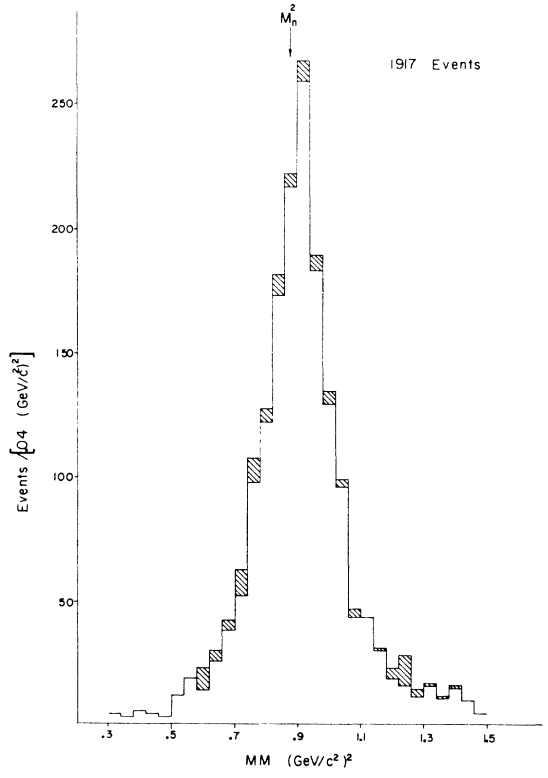

FIG. 20. Unfitted neutron mass squared from the $p\pi^+\pi^+\pi^-n$ final state. Shaded events are ambiguous with other one-constraint fits.

[45] J. Alitti, J. P. Baton, B. Deler, N. Neveu-René, J. Crussara, J. Ginestet, A. J. Trau, R. Gessaroli, and A. Romano, Phys. Letters **15**, 69 (1965).

[46] P. R. Klein, R. J. Sahni, A. Z. Kovacs, and G. W. Tautfest, Phys. Rev. **150**, 1123 (1966).

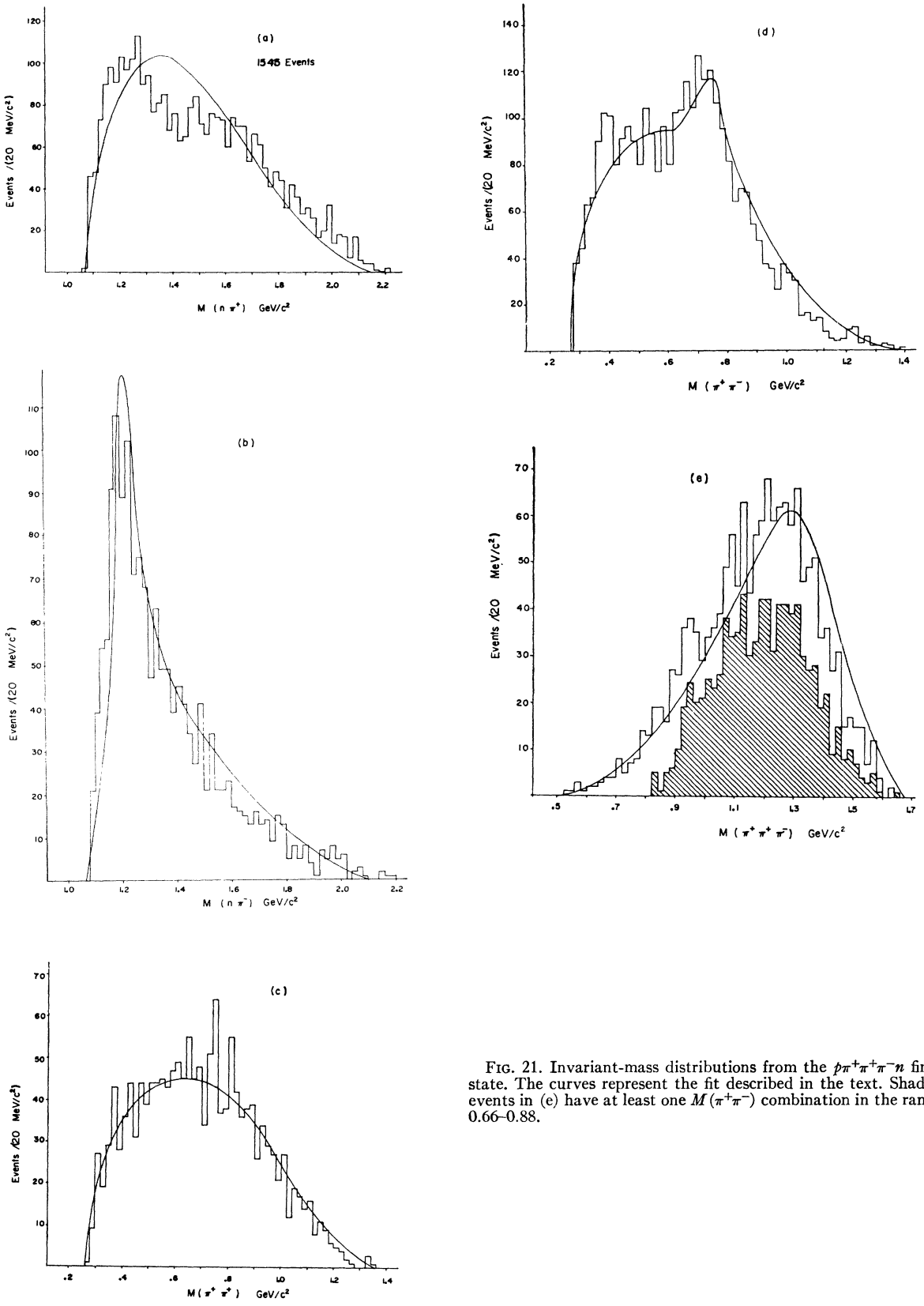

FIG. 21. Invariant-mass distributions from the $p\pi^+\pi^+\pi^-n$ final state. The curves represent the fit described in the text. Shaded events in (e) have at least one $M(\pi^+\pi^-)$ combination in the range 0.66–0.88.

TABLE VI. Final-state cross sections. The contributions to σ from events with three and four visible final-state particles are σ_3 and σ_4, respectively. σ_4' is the cross section for events having spectator momentum between 100 and 250 MeV/c.

Final state	σ_3	σ_4	σ_4'	$\sigma_4'/0.24$	σ (mb)
$p_s p\pi^+\pi^-$	2.25±0.21	1.17±0.09	0.83	3.46	3.42±0.30
$p_s p\pi^+\pi^-\pi^0$	2.82±0.26	1.40±0.11	0.98	4.10	4.22±.37
$p_s p\pi^+\pi^-(\geq 2\pi^0)$	1.01±0.14	0.60±0.07	0.39	1.64	1.61±0.21
$p_s\pi^+\pi^+\pi^- n$	1.17±0.12	0.69±0.06	0.50	2.06	1.86±0.18[a]

[a] The corresponding cross sections from $\pi^- p$ experiments are $\sigma(\pi^- p \to n\pi^+\pi^-) = 3.9\pm0.2$ and $\sigma(\pi^- p \to p\pi^+\pi^-\pi^-) = 1.83\pm0.05$ from Refs. 29 and 46, respectively.

There is no obvious structure in the MM distribution, nor is there in the mass spectrum for the system of all of the final-state mesons, Fig. 22(b). However, when the missing mass was required to be near to that of the η (500–600 MeV/c^2), as shown in the shaded figure, evidence was seen for the production of η'. The background curve in Fig. 22(b) is $\eta\pi\pi$ phase space, normalized to the events above 1.0 GeV/c^2. There are approximately 18±5 events above background at about 960 MeV/c^2, which are assumed to come from the decay $\eta' \to \pi^+\pi^-\eta \to \pi^+\pi^-$ neutrals. The mode $\eta' \to \pi^0\pi^0\eta$ also contributes to this final state but is expected to be approximately $\frac{1}{5}$ of the $\pi^+\pi^-\eta$ mode even without the restriction on the mass of the neutrals.

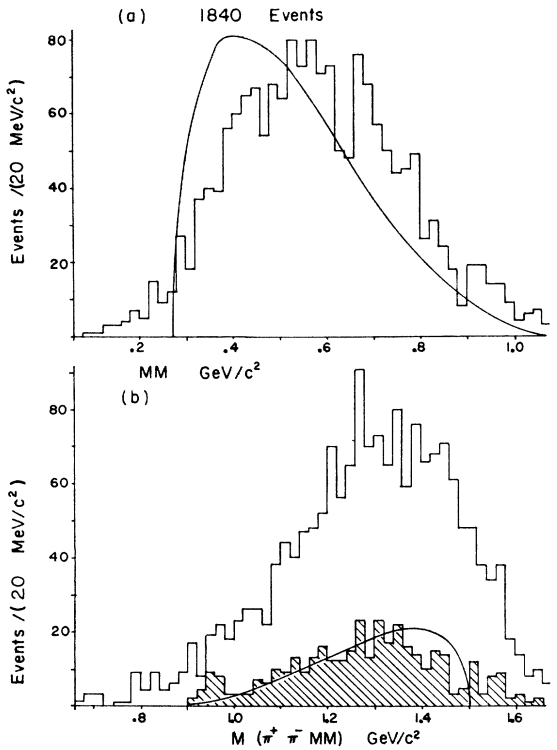

FIG. 22. $pp\pi^+\pi^-$MM final states. (a) Missing mass distribution. The curve is $2\pi^0$ phase space normalized to the total number of events. (b) The mass of the $\pi^+\pi^-$MM combination. The shaded events have $0.5 < \text{MM} < 0.6$. The curve is $\eta\pi\pi$ phase space normalized to the shaded events above 1.0.

IX. CROSS SECTIONS

A. Final-State Cross Sections

The interaction cross section is given by

$$\sigma = N/(pL), \tag{15}$$

where N is the number of interactions which occur for a beam having a total path length L through a material having ρ scattering centers per cm^3.

The number of interactions is basically the number of events found in the scan with two corrections applied. Some of the events which were recorded in the scan should not have been. These included, for example, events with four visible tracks but which had no stopping proton or with secondary interactions on the "spectator" track, events in which the spectator was invisible or too short to be measured in two views (i.e., these should have been recorded as odd-prong events), and events with associated V's. Most of these mistakes were detected and the events were rejected during the measuring. Nevertheless, this correction introduces the largest uncertainty in the cross-section count. The number of events was also corrected for scanning efficiency determined by double scanning some of the film.

In order to determine the total path length of the beam, it was necessary to know the number of beam tracks and the effective length per beam track corresponding to the fiducial criteria of the scan. The beam track count was made from a sample of approximately 2% of the film with restrictions on the direction and curvature of the tracks the same as for the event scan.

The average path length of the beam within the fiducial volume was determined by three methods. The first of these was simply to correct the known fiducial length for camera parallax, track curvature, and absorption of the beam due to the total D_2 cross section. An alternate method was to use the actual distribution of measured events per unit length along the beam direction. This distribution was fitted to $N(y) = N_0 e^{-\sigma\rho y}$, where σ is the total D_2 cross section, ρ is the number of deuterium atoms per cm^3, and N_0 is the intercept of $N(y)$ at the beginning of the fiducial volume. The average track length is then

$$L = \text{number of interactions}/N_0. \tag{16}$$

The third method was to normalize to the total $\pi^+ d$ cross section which is known to better than 1% accuracy at this energy.[47] A special scan of one roll of the film was conducted, where all of the primary interactions within the fiducial volume were recorded as well as the number of beam tracks entering this volume. The three methods gave self-consistent results and the average of

[47] D. V. Bugg, D. C. Salter, G. H. Stafford, R. F. George, K. F. Riley, and R. J. Tapper, Phys. Rev. 146, 980 (1966).

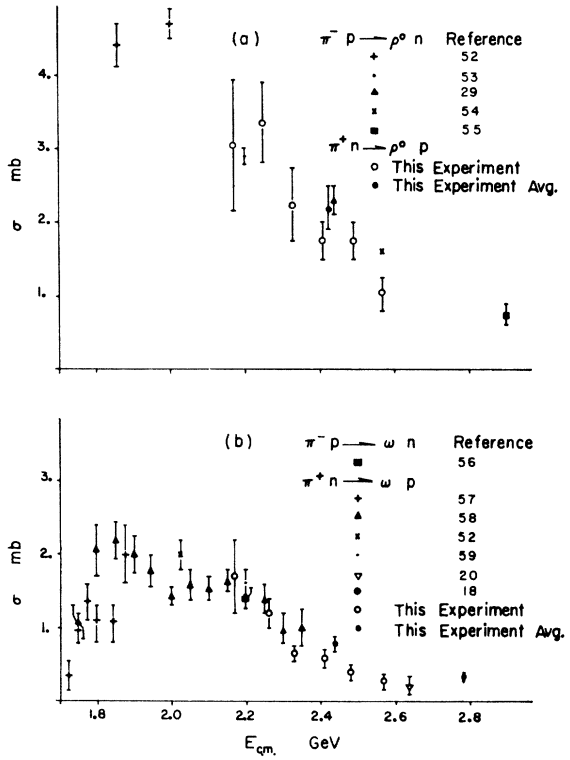

FIG. 23. Energy dependence of the ρ^0 and ω cross sections.

these values was used to calculate the beam path length $L=(1.01\pm0.04)\times10^8$ cm.

The target density ρ has been determined by an experiment at the Lawrence Radiation Laboratory.[48] The standard technique of measuring the track length of the μ^+ emitted in the decay of a stationary π^+ was used.

The cross sections for the final states examined here are listed in Table VI. These numbers have been corrected for the confidence-level cuts on the fits and for the various sources of false fits which have been described in Secs. IV–VII. An alternative method of calculating the cross section, based on visible spectator events only, is also shown. The cross section for events with spectator momentum between 100 and 250 MeV/c was scaled by the expected fraction of these events (0.24) calculated from the Hulthén distribution. The agreement between the two methods is remarkably good.

B. Resonance Cross Sections

Cross sections for some of the resonance production processes leading to the final states observed in this experiment are given in Table VII. All of these values are based on the fits which have been previously described except for the estimated limit on $\pi^+\pi^-\Delta^+$ and $\pi^+\pi^0\Delta^0$. The A-meson cross sections are taken from the fractions, indicated by Fig. 11. The uncertainties are the statistical estimates of the fit combined in quadrature with the uncertainties of the final-state cross sections. It should be realized that the uncertainties associated with the model used in the fitting may also be significant.

The resonance cross sections have been adjusted to include all decay modes using the branching ratios from the compilation of Rosenfeld *et al.*[49]

Where available the comparable cross sections from $\pi^- p$ experiments at this energy are also listed.[50,51] The agreement is generally good.

The impulse model has fairly consistently given a good description of the $\pi^+ d$ interaction. With this justification, the Hulthén wave-function description of the deuteron can be used to extract the energy dependence of the cross sections. Events with spectator momentum between 100 and 250 MeV/c, corresponding to a sample hopefully free from scanning and measuring bias, were used. The results for the reactions $\pi^+ n \to \rho^0 p$ and $\pi^+ n \to \omega p$ are shown in Fig. 23 along with data from some other experiments.[52–59]

ACKNOWLEDGMENTS

It is a pleasure to thank the Lawrence Radiation Laboratory for making the run possible; the cooperation of Dr. J. Kirz, Dr. Donald H. Miller, and Dr. M. Abolins during various phases of the experiment is gratefully acknowledged. We also thank Dr. David Miller for making data tapes of the $\pi^- p$ experiment available to us, Dr. R. Peters, Dr. R. Eisner, and Dr. P. Weisbach for the use of computer programs, and Dr. L. Gutay for helpful discussions. We are also pleased to

[48] P. Hock, University of California Lawrence Radiation Laboratory Physics Note No. 616, 1966 (unpublished).

[49] A. H. Rosenfeld, N. Bavash-Schmidt, A. Barbaro-Galtieri, L. R. Price, P. Soding, C. G. Wohl, M. Roos, and W. J. Willis, Rev. Mod. Phys. **40**, 77 (1968).

[50] O. Guisan, J. Kirz, P. Sonderegger, A. V. Stirling, P. Borgeaud, C. Bruneton, P. Faulk-Vairant, B. Amblard, C. Caversaio, J. P. Guillard, and M. Yvent, Phys. Letters **18**, 200 (1965).

[51] J. Alitti, J. P. Baton, A. Berthelot, B. Deler, W. J. Fickinger, N. Neveu-René, V. Alles-Borelli, R. Gessaroli, A. Romano, and P. Waloschek, Nuovo Cimento **35**, 1 (1965).

[52] T. C. Bacon, W. J. Fickinger, D. G. Hill, H. W. K. Hopkins, D. K. Robinson, and O. E. Salant, in *Proceedings of the Second Topical Conference on Resonant Particles, Athens, Ohio, 1965*, edited by B. A. Munir (Ohio University, Athens, Ohio, 1965), p. 129.

[53] E. West, J. H. Boyd, A. R. Erwin, and W. D. Walker, Phys. Rev. **149**, 1089 (1966).

[54] R. A. Zdanis, L. Madansky, R. W. Kraemer, S. Hertzbach, and R. Strand, Phys. Rev. Letters **14**, 721 (1965).

[55] ABBHLM collaboration, Nuovo Cimento **31**, 729 (1964).

[56] V. V. Barmin, A. G. Dolgolenko, A. G. Meshkivsky, and V. A. Shebanov, Phys. Letters **24B**, 249 (1967).

[57] R. Kraemer, L. Madansky, M. Meer, M. Nussbaum, A. Pevsner, C. Richardson, R. Strand, R. Zdanis, T. Fields, S. Orenstein, and T. Toohig, Phys. Rev. **136**, B496 (1964).

[58] M. Abolins, O. Dahl, J. Danburg, D. Davies, P. Hoch, J. Kirz, D. Miller, and R. Rader, in *Proceedings of the Heidelberg International Conference on Elementary Particles*, edited by H. Filthuth (Wiley-Interscience Publishers, Inc., New York, 1968).

[59] J. H. Boyd, A. R. Erwin, W. D. Walker, and E. West, Phys. Rev. **166**, 1458 (1968).

TABLE VII. Resonance cross sections.

Reaction	σ[a] (mb)	σ from $\pi^- p$	Reference
$\pi^+ n \to \eta p$	0.21±0.04	0.166±0.025[b]	50
$\pi^+ n \to \omega p$	0.80±0.08	...	...
$\pi^+ n \to \rho^0 p$	2.20±0.25	2.3 ±0.2	29
$\pi^+ n \to f^0 p$	0.51±0.20	0.23 ±0.15	29
$\pi^+ n \to A_1^0 p$	0.17±0.10	...	...
$\pi^+ n \to A_2^0 p$	0.14±0.08	...	...
$\pi^+ n \to \eta' p$	0.05±0.02	...	...
$\pi^+ n \to \pi^+ \Delta^0(1238)$	1.8 ±0.2	0.10 ±0.4	29
$\pi^+ n \to \pi^0 \rho^0 p$	0.34±0.07	...	...
$\pi^+ n \to \pi^- \rho^+ p$	0.34±0.07	...	...
$\pi^+ n \to \pi^+ \rho^0 n$	0.43±0.07	0.70 ±0.16	46
		0.36	51
$\pi^+ n \to \pi^+ \pi^+ \Delta^-(1238)$	0.65±0.10	0.77 ±0.08	46
		0.61	51
$\pi^+ n \to \pi^+ \pi^- \Delta^+(1238)$	<0.75	...	...
$\pi^+ n \to \pi^+ \pi^0 \Delta^0(1238)$	<0.75	...	...

[a] The uncertainties quoted are statistical.
[b] At 2.9 GeV/c π^- momentum.

express our appreciation to the technical personnel of the Purdue University High-Energy Group for diligent work in behalf of this experiment.

APPENDIX: CONVENTIONS ASSOCIATED WITH SPECTATOR MODEL OF $\pi^+ d$ INTERACTIONS

The reactions considered can be written $\pi^+ d \to SNX$, where S is the final-state nucleon with the lower three-momentum, N is the other nucleon, and X is any number of final-state mesons. In the impulse approximation the center-of-mass energy was calculated from the final state exclusive of the spectator:

$$E_{\text{c.m.}}^2 = -(P_N + P_x)^2,$$

where P is the four-momentum vector (P_m, iE).

For the generation of Monte Carlo samples, an energy distribution

$$E_{\text{c.m.}}^2 = -(P_\pi + P_d - P_s)^2$$

was used. P_π is the laboratory beam momentum. $P_d = (0,0,0,iM_d)$, and P_s is the momentum of a nucleon with an isotropic three-momentum distributed in magnitude according to the Hulthén function, Eq. (1). The momenta of the other final-state particles were then generated with this center-of-mass energy distribution.

Momentum transfers were calculated from the beam to the appropriate final-state particles. The most usual case, analogous to the momentum transfer to the target in a πp experiment, would be

$$\Delta^2 = (P_\pi - P_x)^2 = (P_d - P_s - P_N)^2.$$

The usual reference axes for decay distributions, in a resonance rest frame, are the beam direction, the direction of the center-of-mass motion, or the target direction. The first case is uniquely defined. For the second case, the direction used was

$$\mathbf{P}_a = \mathbf{P}_N + \mathbf{P}_X,$$

and for the third,

$$\mathbf{P}_a = \mathbf{P}_N + \mathbf{P}_X - \mathbf{P}_\pi.$$